2.2. Plasmids

FLAG-tagged human DDX20-expressing plasmids were kindly provided by Dr. C. Glass and Dr. G. Dreyfuss [8,10]. FLAG-tagged human DDX20-expression plasmids used for generation of DDX20-overexpressing lentiviruses were constructed by inserting the PCR-amplified DDX20 cDNA at the NotI site of the pCDH vector (System Biosciences). Plasmids expressing microRNA precursors (miRNA-22 and miRNA-140 precursors) were purchased from System Biosciences (Mountain View, CA). Reporter plasmids to analyze miRNA function were constructed by inserting annealed synthetic primers containing two tandem sequences, complementary to each miRNA, into the 3′-UTR of the firefly luciferase gene, driven by the CMV promoter (pGL3-basic; Promega, Madison, WI), at the FseI site. Primers used for PCR amplification of DDX20 were: forward, 5′-GCG GCC GCG CCG CCA TGG ACT ACA AGG ACG ACG ACG ACA AGG ACT ACA AGG ACG ACG ACG ACA AGA TGG CGG CGG CAT TTG AAG C-3′ and reverse, 5′-GCG GCC GCT CAC TGG TTA CTA TGC ATC AT TTC-3′. The sequences of the primers used for reporter plasmid construction were as follows: miR-22, 5′-ACA GTT CTT CAA CTG GCA GCT TAA TTA CAG TTC TTC AAC TGG CAG CTT CTC GAG CCG G-3′; miRNA-140–3p, 5′-CCG TGG TTC TAC CCT GTG GTA AAT TCC GTG GTT CTA CCC TGT GGT ACT CGA GCC GG-3′; miRNA-140-5p, 5′-CTA CCA TAG GGT AAA ACC ACT GAA TTC TAC CAT AGG GTA AAA CCA CTG CTC GAG CCG G-3′.

2.3. Lentiviral production and transduction

Cells were transduced with DDX20 (Gemin3)-shRNA and control-shRNA lentiviral particles (Santa Cruz Biotechnology) and then selected on puromycin. To produce FLAG-tagged DDX20 expressing-lentiviruses, 293T cells were transfected with pPACKH1 Packaging Plasmid Mix (System Biosciences) and pCDH-FLAG-tagged DDX20 expressing-lentivector constructs. After 2 days, the supernatants were collected and the viruses were concentrated using PEG-it Virus Precipitation Solution (System Biosciences).

2.4. Transfection and luciferase assay

Transfection was performed using Fugene6 (Promega). Luciferase activities were measured by use of a Dual Luciferase Reporter Assay System (Promega) as described previously [14].

2.5. RNA isolation and reverse transcription

Total RNA was isolated using Trizol Reagent (Invitrogen, Carlsbad, CA). cDNA was synthesized from RNA using the SuperScript III First-Strand Synthesis System (Invitrogen).

2.6. Antibodies

The following antibodies were used: mouse anti-Gemin3 (Ddx20) (sc-57007), rabbit anti-TRADD (sc-7868), rabbit anti-RIP (sc-7881), mouse anti-IKKα (sc-7183), mouse anti-NF-κB p65 (sc-8008), and mouse anti-NF-κB p50 (sc-7188), all purchased from Santa Cruz Biotechnology (Santa Cruz, CA); mouse anti-β-actin (A5316), purchased from Sigma (St. Louis, MO); mouse anti-TRAF2 (#558890) and mouse anti-IKKγ (#559675), purchased from BD Pharmingen (San Diego, CA); rabbit anti-TAK1 (#4505) and rabbit anti-IKKβ (#2370), purchased from Cell Signaling Technology (Danvers, MA); mouse anti-IκBα (#610690), purchased from BD Transduction Laboratories (Lexington, KY); mouse anti-Ago2 (#015-22031) and mouse anti-DYKDDDDY (FLAG)-tag (#018-22381), purchased from Wako (Osaka, Japan).

2.7. Western blotting

Western blotting was performed as described previously [15].

2.8. Reporter plasmids for signal transduction

The following reporter plasmids were used to examine how DDX20 modulated intracellular signaling: pNF-κB-luc, pGAS (IFNγ-activated sequences)-luc, pSRE-luc, pAP-1-luc, and p53-luc were purchased from Stratagene (La Jolla, CA). IL-8-luc, and p3TP-luc (to determine TGFβ pathway activity), were described previously [16]. To construct a reporter plasmid containing mutated NF-κB binding sites, the NF-κB binding motifs, GGGAATTTCC, in pNF-κB-luc were mutated to ATCAATTTCA, as previously reported [17]. Synthetic oligonucleotides with four mutant binding sites (forward, 5′-CTA GCA TCA ATT TCA ATC AAT TTC AAT CAA TTT CAA TCA ATT TCA A-3′; reverse, 5′-GAT CTT GAA ATT GAT TGA AAT TGA TTG AAA TTG ATT GAA ATT GAT G-3′) were annealed and cloned into the NheI and BglII sites of pNF-κB-luc to replace the original NF-κB binding motifs. As positive controls, the following were used: transfection with pFC-MEKK, a MEKK-expressing plasmid, for NF-κB-luc, SRE-luc, and AP-1-luc; transfection with p53-expressing plasmid for p53-luc; incubation for 6 h with 5 ng/mL IFNγ (ProSpec-Tany TechnoGene, Rehovot, Israel) for GAS-luc, and with 5 ng/mL TGFβ (Peprotech, Rocky Hill, NJ) for p3TP-luc.

2.9. EMSA

Nuclear extracts were prepared as described previously [18]. Five micrograms of nuclear extract were incubated with a double-stranded biotin-labeled DNA probe containing NF-κB binding sites (5′-AGT TGA GGG GAC TTT CCC AGG C-3′) plus 1 μg of poly (dI-dC) in a binding buffer (50 mM Tris [pH 7.5], 250 mM NaCl, 2.5 mM DTT, 2.5 mM EDTA, 5 mM $MgCl_2$, and 20% glycerol) at 15 °C for 30 min. DNA–protein complexes were separated on a 6% non-denaturing polyacrylamide gel in 0.5x TBE, and then transferred to nylon membrane (Hybond-N$^+$; GE Healthcare Life Sciences). Oligonucleotides were visualized using the LightShift Chemiluminescent EMSA Kit (Thermo Scientific, Rockford, IL). DNA–protein complex specificity was tested by adding a 100-fold excess of unlabeled (cold) NF-κB probe. To confirm equal loading of nuclear-extracts, the amounts of TFIID, a nuclear protein, were examined by Western blotting using an anti-TFIID antibody (sc-273; Santa Cruz).

2.10. miRNA isolation and quantitation

To measure the amounts of different microRNAs in cells, a Mir-X miRNA qRT-PCR SYBR Kit (Clontech, Mountain View, CA) was used. The levels of U6 snRNA were used for the normalization of cellular miRNA levels. To purify miRNAs from Ago2-related RISCs and DDX20-associated miRNP complexes, microRNAs fractions were isolated using the Human Ago2 MicroRNA Isolation Kit (Wako, Osaka, Japan), which uses antibodies raised to Ago2 and DDX20 to precipitate miRNAs from Ago2-related RISCs and DDX20-associated miRNPs, respectively. The primers used in the quantitative PCR analysis for miRNAs were miRNA-140-5p, CAG TGG TTT TAC CCT ATG GTA G; miRNA-140-3p, TAC CAC AGG GTA GAA CCA CGG; miRNA-22, AAG CTG CCA GTT GAA GAA CTG T.

2.11. Quantitative PCR

Quantitative PCR was performed using the TaqMan Gene Expression system and SYBR Green (Applied Biosystems, Foster City, CA). All target gene expression values were normalized to the expression values for the housekeeping gene, GAPDH, and

relative expression levels were calculated by the $\Delta\Delta C_T$ method: $\Delta\Delta C_T = \Delta C_{Tsample} - \Delta C_{Tgapdh}$ The primers used included (5′–3′): IL-6 forward, CAC AGA CAG CCA CTC ACC TC; IL-6 reverse, TTT TCT GCC AGT GCC TCT TT; IL-8 forward, ATG ACT TCC AAG CTG GCC GTG GCT; IL-8 reverse, TCT CAG CCC TCT TCA AAA ACT TCT C; GAPDH forward, ATC AAC GAC CCC TTC ATT GAC C, and GAPDH reverse, CCA GTA GAC TCC ACG ACA TAC TCA GC.

2.12. Immunoprecipitation

For immunoprecipitation, 293T cells were transfected with FLAG-tagged DDX20-expressing plasmids. FLAG-tagged DDX20 protein was precipitated by incubation with anti-FLAG M2 agarose (Sigma) for 8 h. Cell extracts were prepared as described previously [16].

2.13. Statistical analysis

Statistically significant differences were determined using Student's *t*-test, when variances were equal. When variances were unequal, Welch's *t*-test was instead used.

3. Results

3.1. DDX20 modulates the NF-κB activity

Because it was reported that DDX20 regulates transcriptions [7–9,19], we first examined the effects of altered DDX20 levels on intracellular signaling pathways by a reporter assay (Fig. 1A). While SRE was repressed moderately by DDX20 overexpression consistent with a previous report (Fig. 1A) [8], NF-κB activity was also decreased significantly in our study (Fig. 1A). Thus, we next examined NF-κB activity in stable DDX20-knockdown PLC/PRF/5 cells (Fig. 1B). Whereas DDX20-knockdown cells showed slightly higher NF-κB activity than control cells (Fig. 1C), the response was significantly enhanced by TNFα, which induces NF-κB activity and is involved in the pathogenesis of hepatitis, leading to HCC [20–23] (Fig. 1C). DDX20-knockdown cells consistently showed significantly higher promoter activity for the interleukin (IL)-8 gene, a gene known to be induced by NF-κB [24] (Fig. 1D). To exclude the possibility of cell-specific effects, we established DDX20-knockdown Huh7 cells and observed a similar trend in these cell lines (Supplementary Fig. S1a, b, and c). To further confirm these findings in an overexpression model, we established FLAG-tagged DDX20-overexpressing stable cell lines (Supplementary Fig. S2a). Restoration of NF-κB activity and mRNA levels of IL-6 and IL-8 resulted from DDX20 overexpression, consistent with the results from DDX20-knockdown cells (Supplementary Fig. S2b and c). These results also suggest that DDX20 normally functions to suppress NF-κB activity and the resulting downstream effects of this pathway.

3.2. DDX20 does not modulate or interact with molecules in the NF-κB canonical pathway

To determine how DDX20 deficiency enhances NF-κB activity, we examined the DNA-binding activity of NF-κB, which was increased in DDX20-knockdown cells (Fig. 2A). Although we

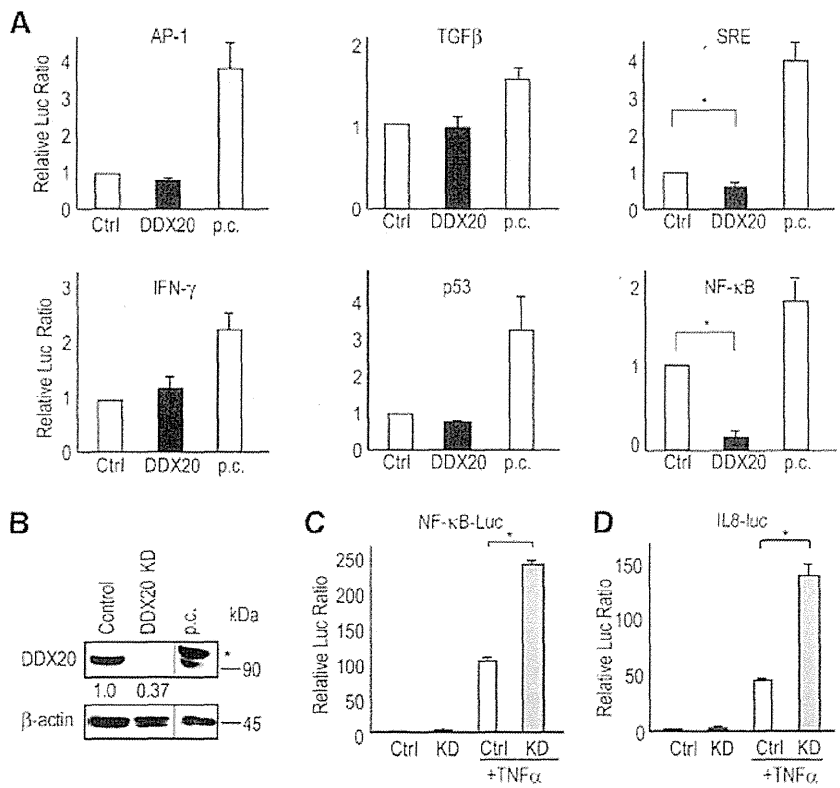

Fig. 1. Modulation of the NF-κB pathway by DDX20. (A) The effects of DDX20 on intracellular signaling pathways as assessed by a reporter assay. Huh7 cells were transiently transfected with a luciferase reporter plasmid and a DDX20-expressing (DDX20) or control plasmid (Ctrl). Luciferase values from control cells were set to 1. The data shown represent the means ± s.d. from at least four independent experiments. p.c.; positive control. (B) Establishment of stable DDX20-knockdown PLC/PRF/5 cells. "FLAG-tagged human DDX20 as a positive control (p.c.). (C, D) Reporter assay data showing that DDX20 deficiency enhances the TNFα-induced activity of NF-κB. Reporter plasmids for NF-κB (C) and its target gene, IL-8 (D), were transiently transfected into control (Ctrl) or DDX20-knockdown (KD) cells. The cells were treated with TNFα (5 ng/mL) or vehicle for 6 h before the reporter assay was performed. "$p < 0.05$. The data shown represent the means ± s.d. from three independent experimental trials. Similar results were obtained in DDX20-knockdown Huh7 cells.

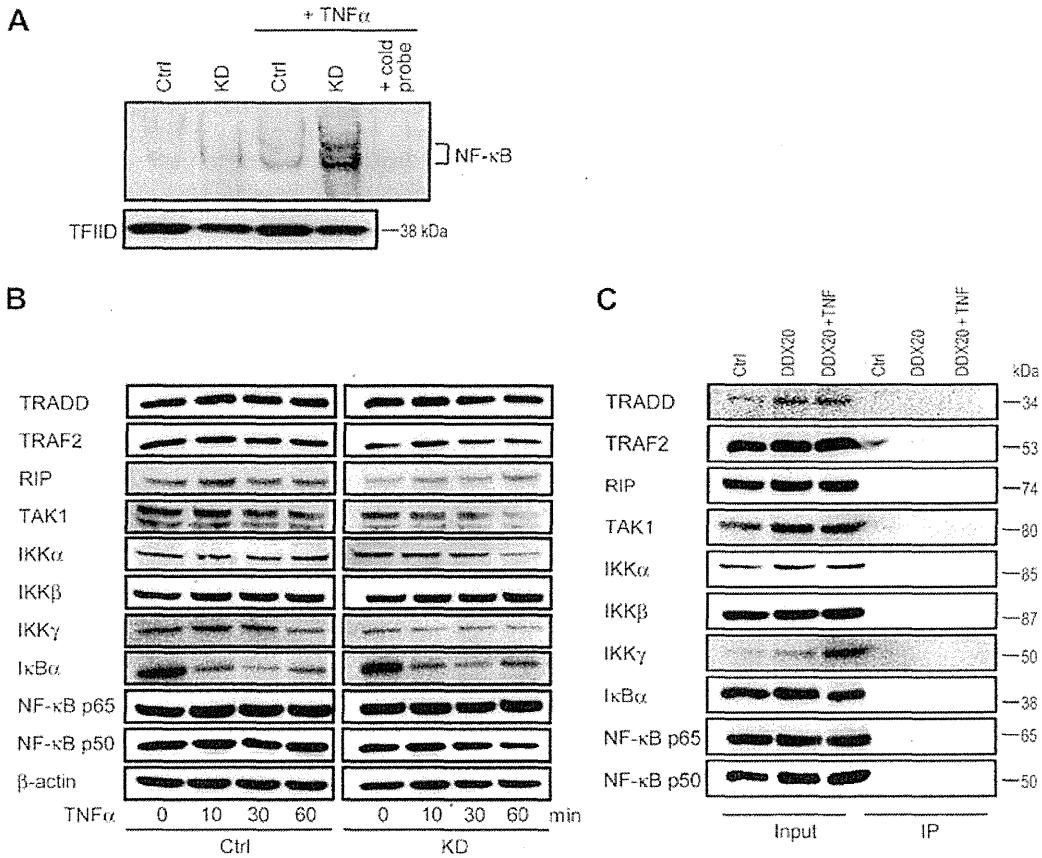

Fig. 2. NF-κB DNA binding is increased in DDX20 knockdown cells after TNFα stimulation. (A) Nuclear extracts from unstimulated and TNFα-stimulated control (Ctrl) and DDX20-knockdown (KD) PLC/PRF/5 cells were analyzed by electrophoretic mobility-shift assay. The specificity of the DNA–protein complex was tested by adding unlabeled NF-κB probe (cold probe) to the TNFα-stimulated KD nuclear extracts. TFIID amounts were examined to confirm equal nuclear extract loading. A representative result is shown from four independent experiments. Similar results were obtained using Huh7 cells. (B) Control (Ctrl) and DDX20-knockdown (KD) PLC/PRF/5 cells were stimulated with 5 ng/mL TNFα for the times indicated. Western blotting was performed using antibodies against the indicated proteins. A representative result is shown from two independent experiments. Similar results were obtained using Huh7 cells. (C) 293T cells (treated with or without 5 ng/mL TNFα for 6 h before the assay) were transfected with a control vector (Ctrl) or a FLAG-tagged DDX20-expressing (DDX20) plasmid. FLAG-tagged DDX20 was immunoprecipitated using anti-FLAG agarose. Co-precipitated proteins were blotted using antibodies against the indicated proteins. Five percent of the total cell lysates were loaded as an input control. Representative results from two independent experiments are shown.

observed IκB-α protein degradation after TNFα stimulation, as expected, the degree of degradation was similar in the control and DDX20-knockdown cells (Fig. 2B) and the levels of the other proteins examined were also similar (Fig. 2B). In addition, we were unable to detect any interactions between DDX20 and the NF-κB pathway-related molecules examined (Fig. 2C). These results suggest that it is unlikely that DDX20 modulates NF-κB activity either by interacting directly with these molecules or by altering their expression levels.

3.3. DDX20 deficiency enhances NF-κB activity by impairing miRNA-140-3p function

Because DDX20 interacts with Ago2 (Fig. 3A), which plays a central role in miRNA function [10,11], we hypothesized that DDX20 deficiency leads to impaired miRNA function and to subsequent activation of NF-κB. Because we previously identified by a comprehensive liver-expressing miRNA library screen that miRNA-22 and miRNA-140 are the critical suppressors of NF-κB activities [25], we hypothesized that DDX20 deficiency enhances NF-κB activity by impairing the NF-κB-suppressing miRNA function.

In DDX20-knockdown cells, the effects of miRNA-140-3p were reduced significantly (Fig. 3B). This impairment of miRNA function had miRNA species-specificity because the degree of functional impairment in DDX20-knockdown cells was much greater for miRNA-140-3p than for miRNA-140-5p and miRNA-22 (Fig. 3B).

While miRNA-22 and miRNA-140 suppressed NF-κB activity in the control cells as we previously reported [25] (Fig. 3C), the suppressive effects of miRNA-140 on NF-κB activity were reduced significantly in DDX20-knockdown cells (Fig. 3C). The reversal of the suppressive effect of miRNA-140 appeared to depend on miRNA-140-3p as miRNA-140-5p showed less functional impairment than did miRNA-140-3p when the corresponding reporter constructs were used as described above (Fig. 3B). The effect was NF-κB specific because no effects were observed for reporters with mutations in the NF-κB binding sites (Fig. 3D).

3.4. DDX20 preferentially interacts with miRNA-140-3p

To elucidate the mechanisms by which DDX20 preferentially impairs certain miRNA functions, we compared the levels of mature miRNAs (miR-22, 140-3p, and 140-5p) in control cells and in DDX20-knockdown cells and found them to be comparable (Fig. 4A). This suggests that DDX20 was not involved in miRNA maturation. We next considered the possibility that the preferential impairment of miRNA function in DDX20-knockdown cells was caused by preferential loading of miRNAs into the RNA-induced silencing complex (RISC). To test this, we immunoprecipitated

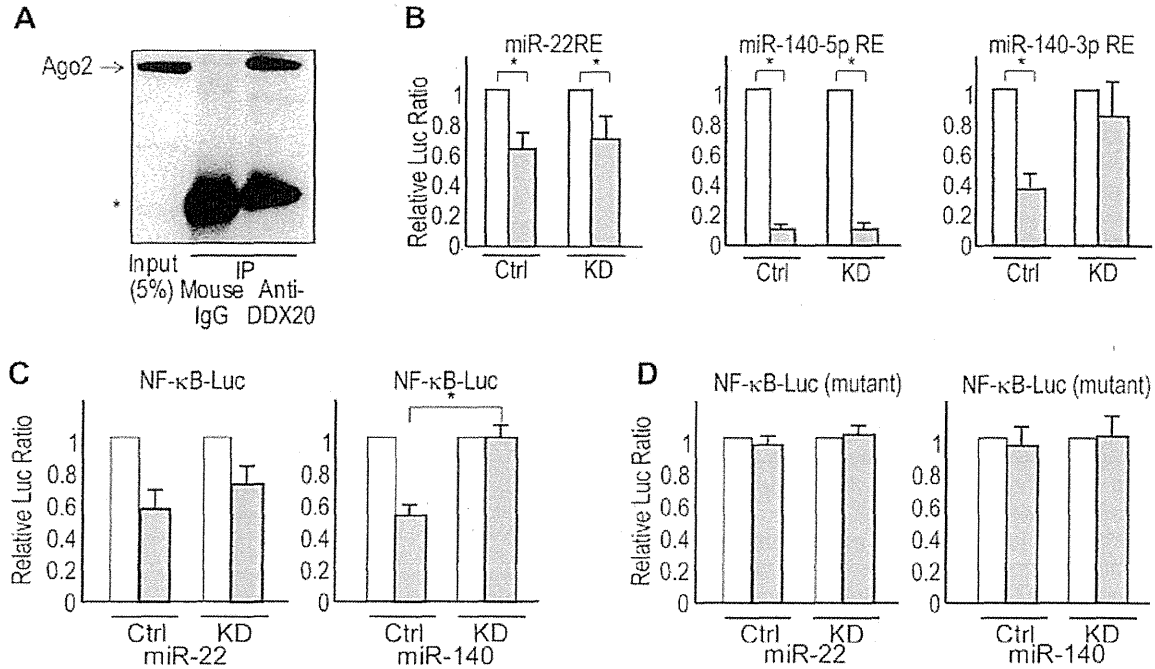

Fig. 3. DDX20 deficiency enhances NF-κB activity by impairing miRNA function. (A) DDX20 binds Ago2. 293T cells were transfected with a FLAG-tagged DDX20-expressing plasmid, and immunoprecipitated using monoclonal antibodies against FLAG-tag or non-immune mouse IgG. Precipitates were blotted with a human anti-Ago2 antibody. Five per cent of each cell lysate was used as an "input" to show the endogenous Ago2 protein. *Bands derived from immunoglobulin light-chain. (B) Overexpression of the miRNA precursors suppresses the activities of the corresponding promoter-reporter constructs in control cells (Ctrl), whereas DDX20 knockdown (DDX KD) reverses the suppressive effects of miRNA-140-3p in PLC/PRF/5 cells. The white and gray bars indicate results with the empty vector and with miRNA precursor overexpression, respectively. $^{*}p < 0.05$. (C) Expression of the miRNA-140 precursor suppresses NF-κB reporter activity in control cells (Ctrl), but this effect was attenuated in DDX20-knockdown PLC/PRF/5 cells (KD) as determined by NF-κB-Luc. The cells were treated with 5 ng/mL TNFα for 6 h. White and gray bars indicate empty vector and miRNA precursor overexpression, respectively. $^{*}p < 0.05$. (D) The suppressive effects by miR-22 and miR-140 were NF-κB-specific. Mutant NF-κB reporter plasmids were transfected with an empty vector (white bar) or the corresponding miRNA precursor-expression plasmids (black bar), into control (Ctrl) and DDX20-knockdown (KD) PLC/PRF/5 cells. Data were normalized and represent the mean ± s.d. of three independent experiments. Similar results were obtained using DDX20-knockdown Huh7 cells.

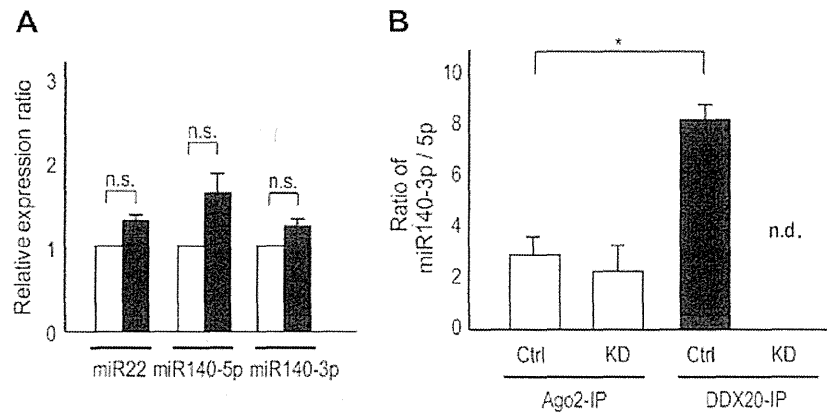

Fig. 4. DDX20 preferentially interacts with miRNA-140-3p. (A) Relative expression of indicated mature miRNAs in the total cellular RNA were measured and normalized to the level of U6 snRNA. The relative ratios of the miRNAs in control cells (white bars) and DDX20-knockdown cells (black bars) were calculated. The data represent the means ± s.d. of six independent experiments. n.s.; non significant. (B) The ratios of miRNA-140-3p to miRNA-140-5p in Ago2- and DDX20-associated RISCs as determined from anti-Ago2 or anti-DDX20 immunoprecipitates (IP) in PLC/PRF/5 control (Ctrl) and DDX20-knockdown (KD) cells. The ratios shown are the means ± s.d. of six independent experiments. Because DDX20-knockdown cells are deficient in DDX20, the anti-DDX20 miRNA ratio was not determined in these cells (n.d.).

Ago2-related RISCs and measured the amount of different miRNAs in the complexes. Because there are no standard small RNAs that can be used as a "house-keeping gene" to adjust for variation in sample loading, we compared miRNA140-5p:miRNA140-3p ratios (since both miRNAs are derived from a single precursor). This ratio in Ago2-related RISCs was approximately two in both control and DDX20-knockdown cells, suggesting that DDX20 was not involved in the preferential loading of specific miRNAs into Ago2-related RISCs (Fig. 4B). However, the ratio in the DDX20-associated miRNPs precipitated from control cells was approximately one to eight (Fig. 4B), indicating that DDX20 preferentially interacts with certain miRNAs, such as miRNA-140-3p, in DDX20-associated miRNPs. The results suggest that functional impairment of certain miRNAs in DDX20-knockdown cells might be caused by the preferential loading of certain miRNAs into DDX20-associated miRNPs. These results further suggest that DDX20 deficiency impairs the function of certain subsets of miRNAs and that this impairment could enhance NF-κB activity by deregulating the NF-κB-suppressive actions of miRNAs, especially miRNA-140-3p, in DDX20-deficient cells.

4. Discussion

Here we report that DDX20 deficiency may enhance NF-κB activities through impairing the NF-κB-suppressing miRNA-140 functions. It was reported that DDX20 is a possible liver tumor suppressor in mice [13]. NF-κB activation is a common feature of human HCCs, particularly those linked to hepatitis [26,27]. In fact, experiments using patient samples suggest that NF-κB activation in the liver leads to the development of HCC [28]. Taken together, these results suggest that the enhancement of NF-κB activity that occurs when DDX20 is deficient may play a role on hepatocarcinogenesis.

Our results indicate that, although DDX20 is one of the major components of Ago2-related RISCs, which play central roles in global miRNA functions [10], impairment of miRNA function due to DDX20 deficiency appears to be miRNA species-specific at the point of loading miRNAs into RISCs. While the precise mechanisms how DDX20 preferentially loads specific miRNAs into RISCs remain to be elucidated, because not all miRNPs have the same components, variation in RISC complexes may determine the properties or specificities of individual miRNAs [10].

Because DDX20 is a multifunctional protein, the miRNA functional impairment reported in the present study may not be the only consequence of DDX20 deficiency. In addition, because novel miRNAs are continually being discovered, other currently unknown miRNAs may also be involved in the biologic role of DDX20. Nonetheless, this study shows that DDX20 is involved in the function of specific miRNAs and the resulting control of NF-κB activity. These results suggest that it is important to investigate not only aberrant miRNA expression levels [29–32] but also deregulation of miRNP components with the subsequent impairment of miRNA function as a path of pathogenesis in human diseases.

Acknowledgments

We thank G. Dreyfuss, and C.K. Glass for providing materials. This work was supported by Grants-in-Aid from the Ministry of Education, Culture, Sports, Science and Technology, Japan (#22390058, #23590960, #17016016, and #20390204) (M. Otsuka, T.G., M. Omata, and K. Koike); by Health Sciences Research Grants from the Ministry of Health, Labor and Welfare of Japan (Research on Hepatitis) (to K. Koike).

Appendix A. Supplementary data

Supplementary data associated with this article can be found, in the online version, at http://dx.doi.org/10.1016/j.bbrc.2012.03.034.

References

[1] D. Parkin, F. Bray, J. Ferlay, P. Pisani, Global cancer statistics, 2002, CA Cancer, J. Clin. 55 (2005) 74–108.

[2] H. El-Serag, Epidemiology of hepatocellular carcinoma in USA, Hepatol. Res. 37 (Suppl.2) (2007) S88–94.

[3] J. Llovet, J. Bruix, Molecular targeted therapies in hepatocellular carcinoma, Hepatology 48 (2008) 1312–1327.

[4] J. Llovet, S. Ricci, V. Mazzaferro, P. Hilgard, E. Gane, J. Blanc, A. de Oliveira, A. Santoro, J. Raoul, A. Forner, M. Schwartz, C. Porta, S. Zeuzem, L. Bolondi, T. Greten, P. Galle, J. Seitz, I. Borbath, D. Häussinger, T. Giannaris, M. Shan, M. Moscovici, D. Voliotis, J. Bruix, S.I.S. Group, Sorafenib in advanced hepatocellular carcinoma, N. Engl. J. Med. 359 (2008) 378–390.

[5] M. Voss, A. Hille, S. Barth, A. Spurk, F. Hennrich, D. Holzer, N. Mueller-Lantzsch, E. Kremmer, F. Grässer, Functional cooperation of Epstein-Barr virus nuclear antigen 2 and the survival motor neuron protein in transactivation of the viral LMP1 promoter, J. Virol. 75 (2001) 11781–11790.

[6] B. Charroux, L. Pellizzoni, R. Perkinson, A. Shevchenko, M. Mann, G. Dreyfuss, Gemin3: a novel DEAD box protein that interacts with SMN, the spinal muscular atrophy gene product, and is a component of gems, J. Cell. Biol. 147 (1999) 1181–1194.

[7] Q. Ou, J. Mouillet, X. Yan, C. Dorn, P. Crawford, Y. Sadovsky, The DEAD box protein DP103 is a regulator of steroidogenic factor-1, Mol. Endocrinol. 15 (2001) 69–79.

[8] G. Klappacher, V. Lunyak, D. Sykes, D. Sawka-Verhelle, J. Sage, G. Brard, S. Ngo, D. Gangadharan, T. Jacks, M. Kamps, D. Rose, M. Rosenfeld, C. Glass, An induced Ets repressor complex regulates growth arrest during terminal macrophage differentiation, Cell 109 (2002) 169–180.

[9] A. Gillian, J. Svaren, The Ddx20/DP103 dead box protein represses transcriptional activation by Egr2/Krox-20, J. Biol. Chem. 279 (2004) 9056–9063.

[10] Z. Mourelatos, J. Dostie, S. Paushkin, A. Sharma, B. Charroux, L. Abel, J. Rappsilber, M. Mann, G. Dreyfuss, MiRNPs: a novel class of ribonucleoproteins containing numerous microRNAs, Genes Dev. 16 (2002) 720–728.

[11] G. Hutvágner, P. Zamore, A MicroRNA in a multiple-turnover RNAi enzyme complex, Science 297 (2002) 2056–2060.

[12] J. Mouillet, X. Yan, Q. Ou, L. Jin, L. Muglia, P. Crawford, Y. Sadovsky, DEAD-box protein-103 (DP103, Ddx20) is essential for early embryonic development and modulates ovarian morphology and function, Endocrinology 149 (2008) 2168–2175.

[13] L. Zender, W. Xue, J. Zuber, C. Semighini, A. Krasnitz, B. Ma, P. Zender, S. Kubicka, J. Luk, P. Schirmacher, W. McCombie, M. Wigler, J. Hicks, G. Hannon, S. Powers, S. Lowe, An oncogenomics-based in vivo RNAi screen identifies tumor suppressors in liver cancer, Cell 135 (2008) 852–864.

[14] M. Otsuka, Q. Jing, P. Georgel, L. New, J. Chen, J. Mols, Y.J. Kang, Z. Jiang, X. Du, R. Cook, S.C. Das, A.K. Pattnaik, B. Beutler, J. Han, Hypersusceptibility to vesicular stomatitis virus infection in Dicer1-deficient mice is due to impaired miR24 and miR93 expression, Immunity 27 (2007) 123–134.

[15] M. Otsuka, A. Takata, T. Yoshikawa, K. Kojima, T. Kishikawa, C. Shibata, M. Takekawa, H. Yoshida, M. Omata, K. Koike, Receptor for activated protein kinase C: requirement for efficient microRNA function and reduced expression in hepatocellular carcinoma, PLoS One 6 (2011) e24359.

[16] M. Otsuka, N. Kato, K. Lan, H. Yoshida, J. Kato, T. Goto, Y. Shiratori, M. Omata, Hepatitis C virus core protein enhances p53 function through augmentation of DNA binding affinity and transcriptional ability, J. Biol. Chem. 275 (2000) 34122–34130.

[17] J. Miyagawa, M. Muguruma, H. Aoto, I. Suetake, M. Nakamura, S. Tajima, Isolation of the novel cDNA of a gene of which expression is induced by a demethylating stimulus, Gene (1999) 289–295.

[18] E. Schreiber, P. Matthias, M. Müller, W. Schaffner, Rapid detection of octamer binding proteins with 'mini-extracts', prepared from a small number of cells, Nucleic Acids Res. 17 (1989) 6419.

[19] F. Fuller-Pace, A. Jacobs, S. Nicol, Modulation of transcriptional activity of the DEAD-box family of RNA helicases, p68 (Ddx5) and DP103 (Ddx20), by SUMO modification, Biochem. Soc. Trans. 35 (2007) 1427–1429.

[20] T. Luedde, R.F. Schwabe, NF-κB in the liver–linking injury, fibrosis and hepatocellular carcinoma, Nat. Rev. Gastroenterol. Hepatol. 8 (2011) 108–118.

[21] M. Arsura, L. Cavin, Nuclear factor-kappaB and liver carcinogenesis, Cancer Lett. 229 (2005) 157–169.

[22] E. Pikarsky, R. Porat, I. Stein, R. Abramovitch, S. Amit, S. Kasem, E. Gutkovich-Pyest, S. Urieli-Shoval, E. Galun, Y. Ben-Neriah, NF-kappaB functions as a tumour promoter in inflammation-associated cancer, Nature 431 (2004) 461–466.

[23] D. Tai, S. Tsai, Y. Chang, S. Huang, T. Chen, K. Chang, Y. Liaw, Constitutive activation of nuclear factor kappaB in hepatocellular carcinoma, Cancer 89 (2000) 2274–2281.

[24] N. Mukaida, Y. Mahe, K. Matsushima, Cooperative interaction of nuclear factor-kappa B- and cis-regulatory enhancer binding protein-like factor binding elements in activating the interleukin-8 gene by pro-inflammatory cytokines, J. Biol. Chem. 265 (1990) 21128–21133.

[25] A. Takata, M. Otsuka, K. Kojima, T. Yoshikawa, T. Kishikawa, H. Yoshida, K. Koike, MicroRNA-22 and microRNA-140 suppress NF-κB activity by regulating the expression of NF-κB coactivators, Biochem. Biophys. Res. Commun. 411 (2011) 826–831.

[26] T. Block, A. Mehta, C. Fimmel, R. Jordan, Molecular viral oncology of hepatocellular carcinoma, Oncogene 22 (2003) 5093–5107.

[27] M. Karin, Nuclear factor-kappaB in cancer development and progression, Nature 441 (2006) 431–436.

[28] J. Ji, J. Shi, A. Budhu, Z. Yu, M. Forgues, S. Roessler, S. Ambs, Y. Chen, P. Meltzer, C. Croce, L. Qin, K. Man, C. Lo, J. Lee, I. Ng, J. Fan, Z. Tang, H. Sun, X. Wang, MicroRNA expression, survival, and response to interferon in liver cancer, N. Engl. J. Med. 361 (2009) 1437–1447.

[29] K. Kojima, A. Takata, C. Vadnais, M. Otsuka, T. Yoshikawa, M. Akanuma, Y. Kondo, Y.J. Kang, T. Kishikawa, N. Kato, Z. Xie, W.J. Zhang, H. Yoshida, M. Omata, A. Nepveu, K. Koike, MicroRNA122 is a key regulator of α-fetoprotein expression and influences the aggressiveness of hepatocellular carcinoma, Nat. Commun. 2 (2011) 338.

[30] M.S. Kumar, J. Lu, K.L. Mercer, T.R. Golub, T. Jacks, Impaired microRNA processing enhances cellular transformation and tumorigenesis, Nat. Genet. 39 (2007) 673–677.

[31] J. Lu, G. Getz, E.A. Miska, E. Alvarez-Saavedra, J. Lamb, D. Peck, A. Sweet-Cordero, B.L. Ebert, R.H. Mak, A.A. Ferrando, J.R. Downing, T. Jacks, H.R. Horvitz, T.R. Golub, MicroRNA expression profiles classify human cancers, Nature 435 (2005) 834–838.

[32] G. Martello, A. Rosato, F. Ferrari, A. Manfrin, M. Cordenonsi, S. Dupont, E. Enzo, V. Guzzardo, M. Rondina, T. Spruce, A. Parenti, M. Daidone, S. Bicciato, S. Piccolo, A MicroRNA targeting dicer for metastasis control, Cell 141 (2010) 1195–1207.

World Journal of Gastroenterology

Online Submissions: http://www.wjgnet.com/1007-9327office
wjg@wjgnet.com
doi:10.3748/wjg.v18.i12.1385

World J Gastroenterol 2012 March 28; 18(12): 1385-1390
ISSN 1007-9327 (print) ISSN 2219-2840 (online)

BRIEF ARTICLE

Assessment of disease progression in patients with transfusion-associated chronic hepatitis C using transient elastography

Ryota Masuzaki, Ryosuke Tateishi, Haruhiko Yoshida, Toru Arano, Koji Uchino, Kenichiro Enooku, Eriko Goto, Hayato Nakagawa, Yoshinari Asaoka, Yuji Kondo, Tadashi Goto, Hitoshi Ikeda, Shuichiro Shiina, Masao Omata, Kazuhiko Koike

Ryota Masuzaki, Ryosuke Tateishi, Haruhiko Yoshida, Toru Arano, Koji Uchino, Kenichiro Enooku, Eriko Goto, Hayato Nakagawa, Yoshinari Asaoka, Yuji Kondo, Tadashi Goto, Shuichiro Shiina, Kazuhiko Koike, Department of Gastroenterology, Graduate School of Medicine, The University of Tokyo, 1138655 Tokyo, Japan
Hitoshi Ikeda, Department of Clinical Laboratory, The University of Tokyo Hospital, 1138655 Tokyo, Japan
Masao Omata, Yamanashi Prefectural Hospital Organization, 4008506 Yamanashi, Japan
Author contributions: Masuzaki R, Tateishi R and Yoshida H designed research; Masuzaki R, Arano T, Uchino K, Enooku K, Goto E, Nakagawa H, Asaoka Y, Kondo Y and Goto T collected data; Tateishi R and Yoshida H analyzed data; Masuzaki R and Yoshida H wrote the paper; Tateishi R, Ikeda H and Shiina S reviewed the paper; Omata M and Koike K supervised the entire project.
Correspondence to: Dr. Ryota Masuzaki, Department of Gastroenterology, Graduate School of Medicine, The University of Tokyo, 7-3-1 Hongo, Bunkyo-ku, 113-8655 Tokyo, Japan. ryota-m@umin.net
Telephone: +81-3-38155411 Fax: +81-3-38140021
Received: May 12, 2011 Revised: August 1, 2011
Accepted: January 22, 2012
Published online: March 28, 2012

Abstract

AIM: To evaluate the relationship between liver stiffness and duration of infection in blood transfusion-associated hepatitis C virus (HCV) patients with or without hepatocellular carcinoma (HCC).

METHODS: Between December 2006 and June 2008, a total of 524 transfusion-associated HCV-RNA positive patients with or without HCC were enrolled. Liver stiffness was obtained noninvasively by using Fibroscan (Echosens, Paris, France). The date of blood transfusion was obtained by interview. Duration of infection was derived from the interval between the date of blood transfusion and the date of liver stiffness measurement (LSM). Patients were stratified into four groups based on the duration of infection (17-29 years; 30-39 years; 40-49 years; and 50-70 years). The difference in liver stiffness between patients with and without HCC was assessed in each group. Multiple linear regression analysis was used to determine the factors associated with liver stiffness.

RESULTS: A total of 524 patients underwent LSM. Eight patients were excluded because of unsuccessful measurements. Thus 516 patients were included in the current analysis (225 with HCC and 291 without). The patients were 244 men and 272 women, with a mean age of 67.8 ± 9.5 years. The median liver stiffness was 14.3 kPa (25.8 in HCC group and 7.6 in non-HCC group). The patients who developed HCC in short duration of infection were male dominant, having lower platelet count, with a history of heavier alcohol consumption, showing higher liver stiffness, and receiving blood transfusion at an old age. Liver stiffness was positively correlated with duration of infection in patients without HCC (r = 0.132, P = 0.024) but not in patients with HCC (r = -0.103, P = 0.123). Liver stiffness was significantly higher in patients with HCC than in those without in each duration group (P < 0.0001). The factors significantly associated with high liver stiffness in multiple regression were age at blood transfusion (P < 0.0001), duration of infection (P = 0.0015), and heavy alcohol consumption (P = 0.043)

CONCLUSION: Although liver stiffness gradually increases over time, HCC develops in patients with high stiffness value regardless of the duration of infection.

Key words: Transfusion-associated hepatitis C; Transient elastography; Hepatocellular carcinoma; Liver stiffness; Ultrasonography; Liver fibrosis

Peer reviewer: Sebastian Mueller, MD, PhD, Professor of Medicine, Department of Internal Medicine, Salem Medical Center, and Center for Alcohol Research, University of Heidelberg, Zeppelinstraße 11-33, Heidelberg 69121, Germany

Masuzaki R, Tateishi R, Yoshida H, Arano T, Uchino K, Enooku K, Goto E, Nakagawa H, Asaoka Y, Kondo Y, Goto T, Ikeda H, Shiina S, Omata M, Koike K. Assessment of disease progression in patients with transfusion-associated chronic hepatitis C using transient elastography. *World J Gastroenterol* 2012; 18(12): 1385-1390 Available from: URL: http://www.wjgnet.com/1007-9327/full/v18/i12/1385.htm DOI: http://dx.doi.org/10.3748/wjg.v18.i12.1385

INTRODUCTION

Hepatitis C virus (HCV) is a leading cause of chronic liver diseases, presenting serious public health problems worldwide[1,2]. HCV infection generally shows an asymptomatic onset and slow fibrosis progression, with cirrhosis developing after 20-50 years[3-7]. Progression of disease is known to depend on patients' characteristics at the onset of infection[8-12]. Infection at old age, male gender and heavy alcohol consumption are reported to be independently associated with rapid disease progression.

The onset of HCV infection can be reliably estimated in transfusion-associated chronic hepatitis C patients, in contrast to repeating injecting-drug users. In Japan, about 40% of chronic hepatitis C patients and HCV-related HCC patients have a history of blood transfusion typically in 1950s and 1960s[13], when blood supply depended on paid blood donors. Not a few of the blood donors were also injecting-drug users, mainly methamphetamine, among whom HCV spread first after the end of World War II. Viral spread started to decline in Japan after commercial blood banks were entirely abolished in 1969[14].

Chronic hepatitis C with cirrhosis is a strong risk factor for hepatocellular carcinoma (HCC)[15,16]. It has been shown that the risk of HCC increases with the degree of liver fibrosis[17]. Until recently, however, the degree of liver fibrosis could be reliably assessed only with liver biopsy, an invasive procedure with the possibility of serious complications[18,19].

Liver stiffness, which can be noninvasively measured with transient elastography, has been recently reported to be well correlated with histologically assessed liver fibrosis stage[20]. We previously reported that liver stiffness is strongly associated with the risk of HCC[21,22]. The calculated stratum-specific likelihood ratio indicated that the post-test odds for the presence of HCC increase five-fold when liver stiffness is higher than 25 kPa and decrease to one-fifth when lower than 10 kPa. Furthermore, we have confirmed in a prospective study that liver stiffness is a significant risk factor for HCC development, together with male gender, clinical cirrhosis and serum albumin level. However, in those studies we did not fully consider the duration of HCV infection and the age at the onset of infection, which are indicated in several studies to be associated with disease progression.

The aim of this study is to evaluate the association between liver stiffness and the duration of infection in blood transfusion-associated hepatitis C patients with and without HCC, focusing on the risk of HCC development.

MATERIALS AND METHODS

Patients

This study conformed to the ethical guideline of the 1975 Helsinki Declaration and the ethical guidelines for epidemiologic research designed by Japanese Ministry of Education, Culture, Sports, Science and Technology and Ministry of Health, Labor and Welfare. The study design was approved by the ethics committee of the authors' institution. Between December 2006 and June 2008, a total of 1562 patients positive for HCV RNA visited the liver clinic of authors' institution. Among these patients, those with a history of receiving blood transfusion were consecutively enrolled (229 with HCC and 295 without). We excluded from the present study those patients with concomitant hepatitis B virus surface antigen positivity, patients with uncontrollable ascites, patients on interferon therapy, and patients who received multiple blood transfusions.

Transient elastography

Liver stiffness was obtained noninvasively by using Fibroscan (Echosens, Paris, France), a newly developed medical device based on elastometry. Liver stiffness measurement (LSM) was considered valid only when at least eight acquisitions were successful with a success rate of at least 60% and the ratio of inter-quartile range (IQR) to the median value was larger than 30%.

Diagnosis of hepatocellular carcinoma

In patients with HCC, the cancer was diagnosed by dynamic computed tomography (CT), where intrahepatic nodules with hyperattenuation in the arterial phase with washout in the late phase were considered as definite HCC[23,24]. Histopathological diagnosis, using ultrasound-guided biopsy samples, was also performed when required. In patients without HCC, the cancer was ruled out by ultrasonography. No HCC was detected in the subsequent six-month follow-up period among these patients.

Laboratory tests

We determined the following parameters on the day of LSM: serum albumin and total bilirubin concentrations, serum aspartate aminotransferase (AST) and alanine aminotransferase (ALT) levels, prothrombin activity and platelet count. Serogrouping of HCV was assessed by enzyme-linked immunosorbent assay (ELISA) (Immucheck F-HCV Gr Kokusai; Sysmex, Kobe, Japan)[25]. Based on the prevalence of each HCV genotype in Japan, serogroup 1 was assumed to represent genotype 1b and serogroup 2 to represent genotype 2a or 2b.

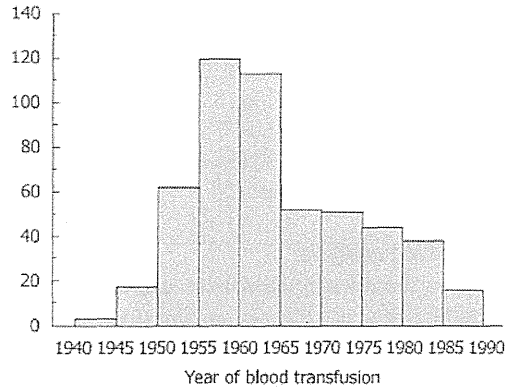

Figure 1 Frequency distribution of the year of receiving blood transfusion among the subjects. There is a peak around the year 1960.

Table 1 Characteristics of patients according to presence of hepatocellular carcinoma *n* (%)

Characteristics	HCC	Non-HCC	*P* value
Overall patients	*n* = 225	*n* = 291	
Gender (M/F)	126/99	118/173	0.0005
Age (yr)[1]	71.2 (66.1-75.7)	68.1 (58.7-72.4)	< 0.0001
Platelet count (10^4/L)[1]	95 (74-133)	161 (111-200)	< 0.0001
ALT (IU/L)[1]	48 (34-68)	42 (25-69)	0.006
Alcohol consumption > 50 g/d	51 (22.7)	28 (9.6)	< 0.0001
Liver stiffness (kPa)[1]	25.8 (17.3-37.4)	7.6 (5.6-13.9)	< 0.0001
IQR (kPa)[1]	4.0 (2.5-6.0)	1.6 (1.2-2.6)	< 0.0001
Duration (17-29 yr)	*n* = 34	*n* = 64	
Gender (M/F)	25/9	38/26	0.0028
Age (yr)[1]	73.1 (65.7-77.1)	59.7 (47.2-69.2)	0.033
Platelet count (10^4/L)[1]	95 (76-154)	180 (116-229)	< 0.0001
ALT (IU/L)[1]	51 (34-89)	42 (22-77)	0.2071
Alcohol consumption > 50 g/d	12 (35.3)	9 (14.1)	0.023
Liver stiffness (kPa)[1]	26.1 (16.8-53.3)	5.9 (4.9-12.1)	< 0.0001
Duration (30-39 yr)	*n* = 40	*n* = 59	
Gender (M/F)	16/24	23/36	0.9191
Age (yr)[1]	72.0 (65.4-76.7)	62.3 (55.7-68.6)	< 0.0001
Platelet count (10^4/L)[1]	93 (68-120)	151 (97-215)	< 0.0001
ALT (IU/L)[1]	42 (33-65)	48 (27-80)	0.7591
Alcohol consumption > 50 g/d	6 (15)	7 (11.9)	0.7641
Liver stiffness (kPa)[1]	28.7 (20.1-37.8)	7.4 (5.7-13.8)	< 0.0001
Duration (40-49 yr)	*n* = 101	*n* = 127	
Gender (M/F)	58/43	51/76	0.0113
Age (yr)[1]	69.2 (65.8-73.6)	69.9 (65.7-72.7)	0.8107
Platelet count (10^4/L)[1]	97 (67-136)	163 (112-195)	< 0.0001
ALT (IU/L)[1]	48 (34-69)	38 (23-64)	0.0080
Alcohol consumption > 50 g/d	25 (24.8)	8 (6.3)	0.0001
Liver stiffness (kPa)[1]	25.1 (17.5-37.4)	8.2 (5.8-14.1)	< 0.0001
Duration (50-70 yr)	*n* = 50	*n* = 41	
Gender (M/F)	27/23	18/23	0.4016
Age (yr)[1]	74.4 (70.0-78.1)	73.7 (66.3-79.2)	0.5658
Platelet count (10^4/L)[1]	97 (81-141)	147 (117-189)	0.0001
ALT (IU/L)[1]	52 (36-69)	46 (32-63)	0.1700
Alcohol consumption > 50 g/d	8 (16)	4 (9.8)	0.5363
Liver stiffness (kPa)[1]	16.0 (8.0-36.3)	7.9 (6.5-15.8)	< 0.0001

[1]Data are expressed as median (25th-75th percentiles). ALT: Alanine aminotransferase; IQR: Inter-quartile range; HCC: Hepatocellular carcinoma; M: Male; F: Female.

Duration of infection and liver stiffness progression

The date of blood transfusion was obtained by interview. Duration of infection was derived from the interval between the date of blood transfusion and the date of LSM. The rate of liver stiffness progression was calculated as follows: present liver stiffness-minimal stiffness value in the cohort (kPa)/interval after blood transfusion (years).

Statistical analysis

Data were expressed as median and 25th-75th percentiles in parenthesis unless otherwise indicated. The categorical variables were compared by χ^2 tests, whereas continuous variables were compared with unpaired Student's *t* test (parametric) or Mann-Whitney *U* test (non-parametric). A P value < 0.05 on two-tailed test was considered significant.

The correlation between liver stiffness and the interval from blood transfusion was assessed by Spearman's rank correlation. The duration of infection was arbitrarily stratified into 4 groups, 17-29 years; 30-39 years; 40-49 years; and 50-70 years. The difference in liver stiffness according to the presence of HCC was assessed in each group. Multiple linear regression analysis was used to determine the factors associated with liver stiffness. Processing and analysis were performed by using the S-plus Version 7 (TIBCO Software Inc., Palo Alto, CA, United States).

RESULTS

Patients' profile

A total of 524 patients underwent LSM. Eight patients were excluded because of unsuccessful measurements, mostly due to obesity (four patients had IQR/median > 30% and four had a success rate lower than 60%). Thus 516 patients were included in the current analysis (225 with HCC and 291 without). Their characteristics at the time of LSM are summarized in Table 1. The patients were 244 men and 272 women, with a mean age of 67.8 ± 9.5 years. The median liver stiffness was 14.3 kPa (25.8 in HCC group and 7.6 in non-HCC group). Figure 1 shows the frequency distribution of the year of receiving blood transfusion among the subjects. A peak is noted around the year 1960.

Characteristics of patients according to the duration of infection

Characteristics of patients were compared between patients with and without HCC in each duration of infection group (Table 1). The patients who developed HCC in short duration of infection were male dominant, having low platelet count, with a history of heavier alcohol consumption, showing higher liver stiffness, and receiving blood transfusion at an older age.

Correlation between liver stiffness and duration of infection

The correlation between liver stiffness and duration of

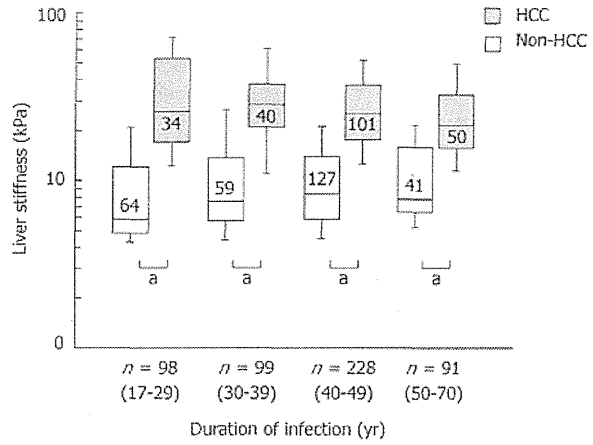

Figure 2 Duration of infection and liver stiffness. Liver stiffness was higher in patients with HCC than in patients without in each infection duration group ($^aP < 0.0001$ by Mann-Whitney *U* test).

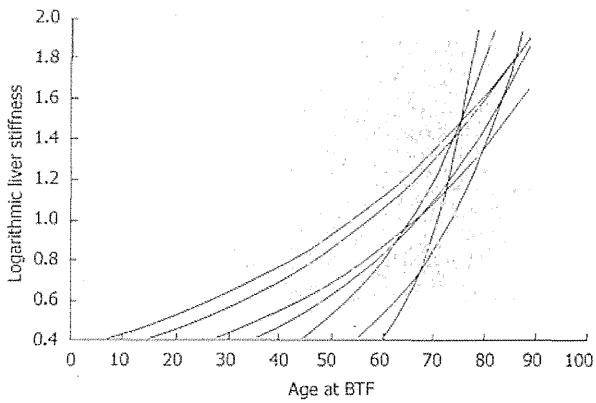

Figure 3 Age at blood transfusion and liver stiffness. Stiffness at present (each dot) and stiffness at BTF (assumed to normal value) were connected approximate logarithmic curve. Stiffness progressions become rapid in older age at BTF.

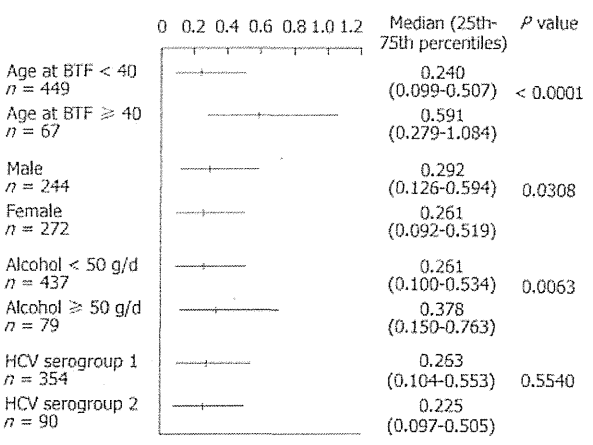

Figure 4 Liver stiffness progression rate. The progression rate is significantly higher in patients who were older than 40 at the time of blood transfusion, whose alcohol consumption is more than 50 g/d, and who are male. There is no significant difference according to hepatitis C virus (HCV) serotypes. Horizontal bar represents median value and 25th-75th percentiles.

infection was significant in patients without HCC ($r = 0.132$, $Z = 2.256$, $P = 0.024$) but not in patients with HCC ($r = -0.103$, $Z = -1.54$, $P = 0.123$). When the duration of infection was stratified into 4 groups, 17-29 years; 30-39 years; 40-49 years; and 50-70 years, liver stiffness was higher in patients with HCC than in patients without in each group ($P < 0.0001$, Figure 2).

Multiple regression analysis

The relationship between present liver stiffness and patients' characteristics, i.e., the age at blood transfusion, duration of infection, gender, and alcohol consumption (alcohol > 50 g/d) was analyzed with multiple linear regression analysis. The results showed that the age at blood transfusion was positively correlated with liver stiffness, with a coefficient of +0.336 per year for kPa, $P < 0.0001$, independently of the duration of infection (coefficient +0.272 per year for kPa, $P = 0.0015$). This suggests that fibrosis progression is more rapid when infection is acquired at older ages. Alcohol consumption was also significantly correlated with a positive coefficient (coefficient +4.183 for kPa, $P = 0.043$).

Stiffness progression and the age at blood transfusion

The progression of liver fibrosis, as represented by the increase in liver stiffness, must have been rapid in patients who have high liver stiffness in spite of short duration of HCV infection. We assumed that the liver stiffness was normal, that is, 2.9 kPa, when patients received blood transfusion. In Figure 3, the slopes represent the estimated increase rates of liver stiffness. In accordance with the results of multiple regression, the estimated increase rate was higher when patients received blood transfusion at older ages.

The progression rate of liver stiffness was assessed in subgroups according to three parameters (Figure 4). The progression rate was significantly higher in patients who were older than 40 at the time of blood transfusion ($P < 0.0001$), which is in accordance with the results of multiple regression. Heavy alcohol consumption (more than 50 g ethanol/d, $P = 0.0308$) and male gender ($P = 0.0063$) also showed significant difference by Mann-Whitney *U* test. There was no significant difference among HCV genotypes.

DISCUSSION

The natural history of chronic hepatitis C concerning liver fibrosis progression has been vigorously studied using liver biopsy specimens. The extent of liver fibrosis is usually evaluated as categorical stages. For example, METAVIR Score uses five stages, F0-F4, for fibrosis evaluation[26]. The fibrosis progression in hepatitis C patients, calculated by using paired liver biopsy, was reported to be 0.1-0.133 Unit per year[12,13]. Liver stiffness measured by transient elastography is now widely accepted as a surrogate marker of liver fibrosis[27]. Liver stiffness is expressed as a continuous variable in kPa unit. The cut-

off for cirrhosis is reportedly 13-17 kPa, and the upper limit of measurement is currently 75 kPa. Thus LSM has a wider dynamic range than histological staging, and the rate of fibrosis progression may be more accurately analyzed with LSM.

In the present study, the increase rate of liver stiffness was positively correlated with the age at blood transfusion, as shown by the steeper slopes of approximation curves when patients received BTF at older ages. The cause of this phenomenon is not clear but age-related changes in immunity may be involved. If this is the case, the increase rate is likely to become higher in the same patient with age. Indeed, each approximation curve in the figure apparently becomes steeper with age, suggesting age-related acceleration. This is to be confirmed in future longitudinal studies.

LSM is useful not only as a surrogate of liver biopsy but also as a risk indicator of HCC development. Indeed, in the present study, liver stiffness is high in patients with HCC regardless of duration of infection. The patients who developed HCC with short duration of infection received blood transfusion at an older age and were older at the time of LSM, male dominant, and showed higher liver stiffness than patients without HCC with similar duration of infection. The difference between patients with and without HCC became smaller with longer duration of infection, as the average liver stiffness in patients with HCC became lower and that in patients without HCC became higher. We speculated that patients with high liver stiffness who received blood transfusion in the early period have already died of HCC or liver failure and were eliminated from the study population. Another possibility is that HCC may develop in patients with relatively low liver stiffness when infection has lasted a long time.

In the present study, the median increase in liver stiffness was calculated as 0.275 kPa per year. Using 13.01 kPa as a cut-off for cirrhosis[28], it will take around 40 years on average to develop cirrhosis, which is consistent with previous reports based on liver biopsy[29]. Admittedly, the present study is basically cross-sectional, and prospective longitudinal LSM will be obviously superior in understanding the natural course of liver fibrosis progression. However, the estimated average increase rate of liver stiffness indicates that such studies will require repeated LSM at an interval of at least five years.

Age at viral infection, alcohol consumption, and male gender were reported to be associated with accelerated fibrosis progression[8-11]. In the present study, we performed subgroup analysis and indeed found that blood transfusion at an age older than 40, male gender, and alcohol consumption more than 50 g ethanol/d were significantly associated with rapid increase in liver stiffness. There is consensus that heavy alcohol consumption is associated with fibrosis progression[30]. Alcohol, which by itself can cause liver disease and fibrosis, may affect liver stiffness and worsen fibrosis in hepatitis C[31]. We did not find a difference in liver stiffness increase rate between HCV genotypes 1 (mostly 1b) and 2 (2a/2b), although we could not evaluate genotypes 1a, 3 or 4.

This study has some limitations. First, since this is a cross-sectional study performed after LSM became available, patients with more rapid disease progression may have died and been excluded from the study. Second, because transfusion-associated HCV infection has been virtually eliminated in Japan since 1992, we could not include patients with shorter duration of infection. Lastly, we did not perform paired LSM but assumed that liver stiffness was normal at the time of infection. Longitudinal observation is now on-going but will take several years to obtain results.

In conclusion, although liver stiffness gradually increases over time from the onset of infection in general, HCC develops in patients with high liver stiffness regardless of the duration of infection. Patients who acquired HCV infection at older ages showed higher increase rate of liver stiffness and probably more rapid disease progression.

COMMENTS

Background

Liver stiffness, which can be noninvasively measured with transient elastography, has been recently reported to be well correlated with histologically assessed liver fibrosis stage.

Research frontiers

This study evaluated the association between liver stiffness and the duration of infection in blood transfusion-associated hepatitis C patients with and without hepatocellular carcinoma (HCC), focusing on the risk of HCC development.

Innovations and breakthroughs

Liver stiffness is expressed as a continuous variable in kPa unit. The cut-off for cirrhosis is reportedly 13-17 kPa, and the upper limit of measurement is currently 75 kPa. Thus liver stiffness measurement (LSM) has a wider dynamic range than histological staging, and the rate of fibrosis progression may be more accurately analyzed with LSM.

Applications

Although liver stiffness gradually increases over time from the onset of infection in general, HCC develops in patients with high liver stiffness regardless of the duration of infection. Patients who acquired hepatitis C virus (HCV) infection at older ages showed higher increase rate of liver stiffness and probably more rapid disease progression.

Terminology

Transient elastography (Fibro-Scan®; EchoSens, Paris, France) is a rapid, reliable and well-tolerated imaging technique for the assessment of liver fibrosis by measuring liver stiffness.

Peer review

This is an interesting and timely study on liver stiffness in patients with transfusion associatated HCV. The authors show that HCC develops in patients with high liver stiffness regardless of the duration of infection. Patients who acquired HCV infection at older ages showed higher increase rate of liver stiffness. Co-exposure to alcohol is critical. The methodology is sound and the paper is well and clearly written.

REFERENCES

1 **Strader DB**, Wright T, Thomas DL, Seeff LB. Diagnosis, management, and treatment of hepatitis C. *Hepatology* 2004; **39**: 1147-1171

2 **Di Bisceglie AM**. Hepatitis C. *Lancet* 1998; **351**: 351-355

3 **Seeff LB**. The history of the "natural history" of hepatitis C (1968-2009). *Liver Int* 2009; **29** Suppl 1: 89-99

4 **Alberti A**, Chemello L, Benvegnù L. Natural history of hepatitis C. *J Hepatol* 1999; **31** Suppl 1: 17-24

5 **Kiyosawa K**, Sodeyama T, Tanaka E, Gibo Y, Yoshizawa K, Nakano Y, Furuta S, Akahane Y, Nishioka K, Purcell RH. In-

terrelationship of blood transfusion, non-A, non-B hepatitis and hepatocellular carcinoma: analysis by detection of antibody to hepatitis C virus. *Hepatology* 1990; **12**: 671-675

6 **Marcellin P**, Asselah T, Boyer N. Fibrosis and disease progression in hepatitis C. *Hepatology* 2002; **36**: S47-S56

7 **Seeff LB**, Hollinger FB, Alter HJ, Wright EC, Cain CM, Buskell ZJ, Ishak KG, Iber FL, Toro D, Samanta A, Koretz RL, Perrillo RP, Goodman ZD, Knodell RG, Gitnick G, Morgan TR, Schiff ER, Lasky S, Stevens C, Vlahcevic RZ, Weinshel E, Tanwandee T, Lin HJ, Barbosa L. Long-term mortality and morbidity of transfusion-associated non-A, non-B, and type C hepatitis: A National Heart, Lung, and Blood Institute collaborative study. *Hepatology* 2001; **33**: 455-463

8 **Poynard T**, Bedossa P, Opolon P. Natural history of liver fibrosis progression in patients with chronic hepatitis C. The OBSVIRC, METAVIR, CLINIVIR, and DOSVIRC groups. *Lancet* 1997; **349**: 825-832

9 **Matsumura H**, Moriyama M, Goto I, Tanaka N, Okubo H, Arakawa Y. Natural course of progression of liver fibrosis in Japanese patients with chronic liver disease type C--a study of 527 patients at one establishment. *J Viral Hepat* 2000; **7**: 268-275

10 **Hamada H**, Yatsuhashi H, Yano K, Daikoku M, Arisawa K, Inoue O, Koga M, Nakata K, Eguchi K, Yano M. Impact of aging on the development of hepatocellular carcinoma in patients with posttransfusion chronic hepatitis C. *Cancer* 2002; **95**: 331-339

11 **Khan KN**, Yatsuhashi H. Effect of alcohol consumption on the progression of hepatitis C virus infection and risk of hepatocellular carcinoma in Japanese patients. *Alcohol Alcohol* 2000; **35**: 286-295

12 **Minola E**, Prati D, Suter F, Maggiolo F, Caprioli F, Sonzogni A, Fraquelli M, Paggi S, Conte D. Age at infection affects the long-term outcome of transfusion-associated chronic hepatitis C. *Blood* 2002; **99**: 4588-4591

13 **Yoshizawa H**, Tanaka J, Miyakawa Y. National prevention of hepatocellular carcinoma in Japan based on epidemiology of hepatitis C virus infection in the general population. *Intervirology* 2006; **49**: 7-17

14 **Tanaka Y**, Hanada K, Mizokami M, Yeo AE, Shih JW, Gojobori T, Alter HJ. A comparison of the molecular clock of hepatitis C virus in the United States and Japan predicts that hepatocellular carcinoma incidence in the United States will increase over the next two decades. *Proc Natl Acad Sci USA* 2002; **99**: 15584-15589

15 **Masuzaki R**, Yoshida H, Tateishi R, Shiina S, Omata M. Hepatocellular carcinoma in viral hepatitis: improving standard therapy. *Best Pract Res Clin Gastroenterol* 2008; **22**: 1137-1151

16 **Ikeda K**, Saitoh S, Suzuki Y, Kobayashi M, Tsubota A, Koida I, Arase Y, Fukuda M, Chayama K, Murashima N, Kumada H. Disease progression and hepatocellular carcinogenesis in patients with chronic viral hepatitis: a prospective observation of 2215 patients. *J Hepatol* 1998; **28**: 930-938

17 **Yoshida H**, Shiratori Y, Moriyama M, Arakawa Y, Ide T, Sata M, Inoue O, Yano M, Tanaka M, Fujiyama S, Nishiguchi S, Kuroki T, Imazeki F, Yokosuka O, Kinoyama S, Yamada G, Omata M. Interferon therapy reduces the risk for hepatocellular carcinoma: national surveillance program of cirrhotic and noncirrhotic patients with chronic hepatitis C in Japan. IHIT Study Group. Inhibition of Hepatocarcinogenesis by Interferon Therapy. *Ann Intern Med* 1999; **131**: 174-181

18 **Dienstag JL**. The role of liver biopsy in chronic hepatitis C. *Hepatology* 2002; **36**: S152-S160

19 **Bedossa P**, Dargère D, Paradis V. Sampling variability of liver fibrosis in chronic hepatitis C. *Hepatology* 2003; **38**: 1449-1457

20 **Castéra L**, Vergniol J, Foucher J, Le Bail B, Chanteloup E, Haaser M, Darriet M, Couzigou P, De Lédinghen V. Prospective comparison of transient elastography, Fibrotest, APRI, and liver biopsy for the assessment of fibrosis in chronic hepatitis C. *Gastroenterology* 2005; **128**: 343-350

21 **Masuzaki R**, Tateishi R, Yoshida H, Goto E, Sato T, Ohki T, Imamura J, Goto T, Kanai F, Kato N, Ikeda H, Shiina S, Kawabe T, Omata M. Prospective risk assessment for hepatocellular carcinoma development in patients with chronic hepatitis C by transient elastography. *Hepatology* 2009; **49**: 1954-1961

22 **Masuzaki R**, Tateishi R, Yoshida H, Yoshida H, Sato S, Kato N, Kanai F, Sugioka Y, Ikeda H, Shiina S, Kawabe T, Omata M. Risk assessment of hepatocellular carcinoma in chronic hepatitis C patients by transient elastography. *J Clin Gastroenterol* 2008; **42**: 839-843

23 **Makuuchi M**, Kokudo N, Arii S, Futagawa S, Kaneko S, Kawasaki S, Matsuyama Y, Okazaki M, Okita K, Omata M, Saida Y, Takayama T, Yamaoka Y. Development of evidence-based clinical guidelines for the diagnosis and treatment of hepatocellular carcinoma in Japan. *Hepatol Res* 2008; **38**: 37-51

24 **Kudo M**, Okanoue T. Management of hepatocellular carcinoma in Japan: consensus-based clinical practice manual proposed by the Japan Society of Hepatology. *Oncology* 2007; **72** Suppl 1: 2-15

25 **Moriyama M**, Matsumura H, Nirei K, Arakawa Y, Yamagami H, Ogawa M, Kaneko M, Matsuoka S, Amaki S, Tanaka N, Arakawa Y. Factors influencing treatment efficacy of 24-week combination therapy with interferon alpha-2b plus ribavirin for chronic hepatitis C. *Dig Dis Sci* 2007; **52**: 2418-2426

26 **Bedossa P**, Poynard T. An algorithm for the grading of activity in chronic hepatitis C. The METAVIR Cooperative Study Group. *Hepatology* 1996; **24**: 289-293

27 **Ghany MG**, Kleiner DE, Alter H, Doo E, Khokar F, Promrat K, Herion D, Park Y, Liang TJ, Hoofnagle JH. Progression of fibrosis in chronic hepatitis C. *Gastroenterology* 2003; **124**: 97-104

28 **Friedrich-Rust M**, Ong MF, Martens S, Sarrazin C, Bojunga J, Zeuzem S, Herrmann E. Performance of transient elastography for the staging of liver fibrosis: a meta-analysis. *Gastroenterology* 2008; **134**: 960-974

29 **Shiratori Y**, Imazeki F, Moriyama M, Yano M, Arakawa Y, Yokosuka O, Kuroki T, Nishiguchi S, Sata M, Yamada G, Fujiyama S, Yoshida H, Omata M. Histologic improvement of fibrosis in patients with hepatitis C who have sustained response to interferon therapy. *Ann Intern Med* 2000; **132**: 517-524

30 EASL International Consensus Conference on Hepatitis C. Paris, 26-28, February 1999, Consensus Statement. European Association for the Study of the Liver. *J Hepatol* 1999; **30**: 956-961

31 **Mueller S**, Millonig G, Sarovska L, Friedrich S, Reimann FM, Pritsch M, Eisele S, Stickel F, Longerich T, Schirmacher P, Seitz HK. Increased liver stiffness in alcoholic liver disease: differentiating fibrosis from steatohepatitis. *World J Gastroenterol* 2010; **16**: 966-972

S- Editor Shi ZF **L- Editor** O'Neill M **E- Editor** Xiong L

Cancer Science
The official journal of the Japanese Cancer Association JCA

Loss of 5-hydroxymethylcytosine is accompanied with malignant cellular transformation

Yotaro Kudo,[1] Keisuke Tateishi,[1,3] Keisuke Yamamoto,[1] Shinzo Yamamoto,[1] Yoshinari Asaoka,[1] Hideaki Ijichi,[1] Genta Nagae,[2] Haruhiko Yoshida,[1] Hiroyuki Aburatani[2] and Kazuhiko Koike[1]

[1]Department of Gastroenterology, Graduate School of Medicine, and [2]Genome Science Division, Research Center for Advanced Science and Technology, University of Tokyo, Tokyo, Japan

(Received October 17, 2011/Revised December 21, 2011/Accepted January 3, 2012/Accepted manuscript online February 9, 2012/Article first published online February 27, 2012)

Dysregulated DNA methylation followed by abnormal gene expression is an epigenetic hallmark in cancer. DNA methylation is catalyzed by DNA methyltransferases, and the aberrant expression or mutations of DNA methyltransferase genes are found in human neoplasm. The enzymes for demethylating 5-methylcytosine were recently identified, and the biological significance of DNA demethylation is a current focus of scientific attention in various research fields. Ten–eleven translocation (TET) proteins have an enzymatic activity for the conversion from 5-methylcytosine to 5-hydroxymethylcytosine (5-hmC), which is an intermediate of DNA demethylation. The loss-of-function mutations of *TET2* gene were reported in myeloid malignancies, suggesting that impaired TET-mediated DNA demethylation could play a crucial role in tumorigenesis. It is still unknown, however, whether DNA demethylation is involved in biological properties in solid cancers. Here, we show the loss of 5-hmC in a broad spectrum of solid tumors: for example, a significant reduction of 5-hmC was found in 72.7% of colorectal cancers (CRCs) and 75% of gastric cancers compared to background tissues. *TET1* expression was decreased in half of CRCs, and a large part of them was followed by the loss of 5-hmC. These findings suggest that the amount of 5-hmC in tumors is often reduced via various mechanisms, including the downregulation of *TET1*. Consistently, in the *in vitro* experiments, the downregulation of *TET1* was clearly induced by oncogene-dependent cellular transformation, and loss of 5-hmC was seen in the transformed cells. These results suggest the critical roles of aberrant DNA demethylation for oncogenic processes in solid tissues. (*Cancer Sci* 2012; 103: 670–676)

Patterns of DNA methylation, histone modification and chromatin structure are profoundly altered in human cancers.[1–5] In particular, aberrant promoter hypermethylation leading to inappropriate transcriptional silencing of genes, especially tumor suppressor genes, is often found in various types of human neoplasm, including colorectal and gastric cancers.[6–9] DNA methylation is catalyzed by DNA methyltransferases (DNMTs), and it is reported that the increased level of DNMT1 is correlated with the histological grade or poor prognosis of human cancers.[10–12] In addition, a recent report demonstrated somatic mutations in the *DNMT3A* gene from acute myeloid leukemia patients.[13]

Global loss of methylated DNA in paternal genome after fertilization suggests active DNA demethylation pathway in mammalian cells, although the molecular mechanism has been unknown for a long time. The recent discovery of ten–eleven translocation (TET) proteins those are capable of converting from 5-methylcytosine to 5-hydroxymethylcytosine (5-hmC) gave a breakthrough to the epigenetic research field.[14–19] Following studies showed that the activation-induced cytidine deaminase family convert cytosine to uracil and 5-hmC to 5-hydroxymethyluracil,[20,21] and that TET1 mediates further oxidation of 5-hmC to 5-formylcytosine and 5-carboxylcytosine.[17,18] These reports indicate that the active DNA demethylation may be established through multiple steps generating various forms of intermediates.[22]

5-hydroxymethylcytosine (5-hmC), a proposed intermediate of DNA demethylation, is abundant in embryonic stem (ES) cells and adult neural cells.[15,23–25] Accordingly, 5-hmC and TET proteins have been vigorously discussed from the aspect of cellular differentiation and pluripotency of ES cells.[15,23] Meanwhile, the biological significance of 5-hmC and TETs remains elusive in human cancers. It was recently reported that myeloid cancers have the mutations of *TET2* gene compromising the catalytic activity and show the lower levels of 5-hmC.[26–29] In contrast, in human solid cancers, biological significance of TETs and 5-hmC remains elusive. A recent study revealed that 5-hmC levels were decreased in solid tumors compared to normal tissues by immunohistochemistry;[30] however, there was no analysis comparing the 5-hmC levels among matched-pair samples.

Here, we semiquantitatively demonstrate the reduced level of 5-hmC in human cancers by examining paired matched tissues. In addition, we found that the *TET1* mRNA is suppressed under oncogene-induced cellular transformation, resulting in loss of 5-hmC.

Materials and Methods

Immunostaining. All procedures involving animals were approved by the institutional committee for animal research at the University of Tokyo and complied with the Guide for the Care and Use of Laboratory Animals. A frozen acetone-fixed tumor and normal tissue arrays were purchased from BioChain (Hayward, CA, USA). Slides were treated with 2 M hydrochloric acid followed by blocking with 10% goat serum in PBS for 1 h at room temperature and incubated with primary anti-5-hmC polyclonal antibody (1:10 000; Active Motif, Carlsbad, CA, USA) in 1% goat serum and 0.1% Triton X-100 in PBS at 4°C overnight, and were further labeled with secondary antibodies conjugated with Alexa 488 dyes (Invitrogen, Tokyo, Japan). Cell nuclei were counterstained with Hoechst 33342 dye (Dojindo, Kumamoto, Japan). All florescent images were taken using an Olympus AX80 microscope (Olympus, Tokyo, Japan).

Clinical human tissue samples. A total of 22 colorectal and 12 gastric adenocarcinoma samples were obtained from Motojima General Hospital (Gumma, Japan). All patients gave

[3]To whom correspondence should be addressed.
E-mail: ktate-tky@umin.ac.jp

doi: 10.1111/j.1349-7006.2012.02213.x

informed consent prior to specimen collection, and the study was approved by the medical ethics committee.

DNA samples and dot blot analysis. Genomic DNA samples were collected from frozen surgical specimens or cultured cells using a QIAamp DNA Mini Kit (Qiagen, Tokyo, Japan) according to the manufacturer's instructions. Unmethylated, 5-mC-DNA and 5-hmC-DNA standard samples were purchased from Active Motif.

Genomic DNA samples were prepared in 0.1 M NaOH and denatured at 95°C for 5 min, then placed on ice, and neutralized with 0.1 volume of 6.6 M ammonium acetate. The samples were spotted onto Hybond-N+ nylon membrane (GE Healthcare, Tokyo, Japan), fixed with UV irradiation (Stratalinker 1800, auto crosslink-mode; Stratagene, Tokyo, Japan), washed, blocked with 5% skim milk, and incubated with anti-5-hmC antibody (1:10 000) or anti-5-mC monoclonal antibody (5 μg/mL; Calbiochem, Tokyo, Japan) at 4°C overnight, followed by incubation with species-specific HRP-conjugated secondary antibody (1:2000), and dot signal was visualized with the ECL Plus chemiluminescence assay kit (GE Healthcare). To ensure equal spotting of total DNA on the membrane, the same blot was stained with 0.02% methylene blue in 0.3 M sodium acetate (pH 5.2).

Quantitative real-time RT-PCR. Total RNA was extracted from cells using the Fast-Pure RNA Kit (Takara Bio, Shiga, Japan) or from clinical specimens using ISOGEN (Nippon Gene, Tokyo, Japan). Complementary DNA (cDNA) was synthesized

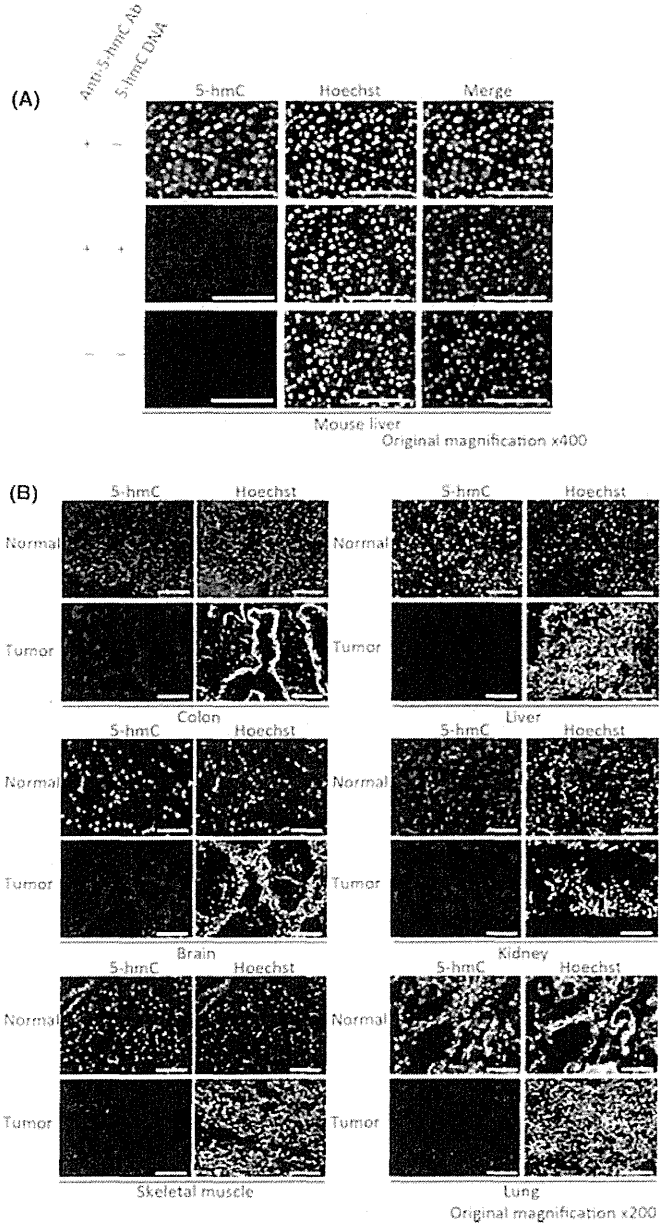

Fig. 1. Immunostaining of 5-hmC. Mouse liver tissues (A) and human tissue arrays (B) were stained with anti-5-hmC (green) antibody or Hoechst 33342 (blue). Scale bar: 100 μm.

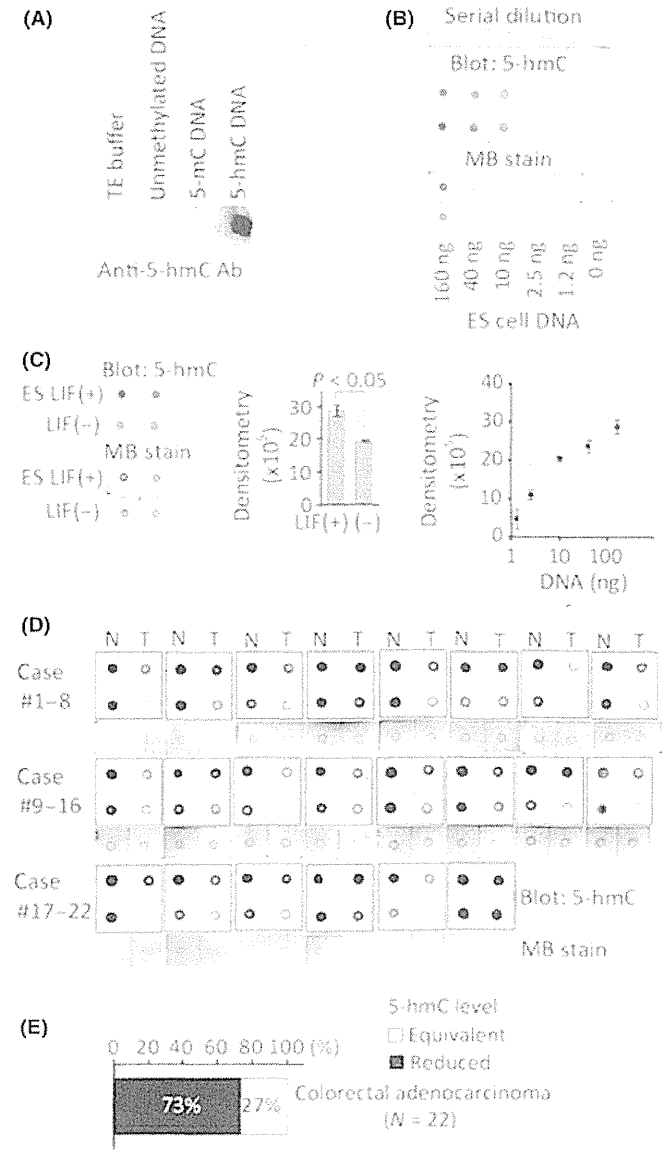

Fig. 2. Measurement of 5-hmC in colorectal cancers (CRCs). (A) Dot blot analysis using anti-5hmC antibody. (B) Genomic DNA from embryonic stem (ES) cells was subjected to dot blot. Loading control is shown by the methylene blue (MB) staining. Densitometry measurements against logarithmic DNA amount were plotted. (C) Quantitative assessment of 5-hmC in ES cell DNA (160 ng). ES cells were incubated with or without leukemia inhibitory factor (LIF) for 5 days. (D) Detection of 5-hmC in 22 pairs of clinical CRCs (T; right column on each membrane) and adjacent non-tumorous tissue (N; left) using dot blot. Twofold diluted DNA was also spotted in the second row on the same membrane. Loading control is shown by MB staining of undiluted DNA samples. (E) Classification of CRCs according to the 5-hmC level.

using the ImProm II reverse transcription system (Promega, Tokyo, Japan) and then subjected to quantitative RT-PCR with the ABI Prism 7000 Sequence Detection System (Applied Biosystems, Tokyo, Japan). The levels of gene expression were normalized in relation to that of *β-actin*. The PCR primer sequences are listed in Table S1.

Mutational analysis. Mutational analysis of *KRAS* exon1 and *BRAF* exon15 were performed using PCR (primers used to amplify those loci are described in Table S2) and direct sequencing methods as described previously.[31]

Cell lines and lentiviral-mediated *Tet1* knockdown. NIH3T3-$BRAF^{V600E}$ cells were generated by transfection of human $BRAF^{V600E}$, as previously described.[32] Lentiviral short hairpin RNA vectors were purchased from Open Biosystems (Huntsville, AL, USA). NIH3T3 cells were infected with the virus according to the manufacturer's protocol and selected by puromycin.

Basic fibroblast growth factor treatment and immunoblot analysis. NIH3T3 cells were serum-starved for 24 h followed by basic fibroblast growth factor (bFGF; 1 μg/mL) stimulation for 30 min, and then lysed directly in Laemmli buffer. Blots were probed with anti-phospho-extracellular signal-regulated kinase (Erk) 1/2 (Thr202/Tyr204) or Erk1/2 antibodies (1:1000) followed by incubation with species-specific HRP-conjugated secondary antibodies (1:2000). Proteins were visualized using the ECL Plus chemiluminescence assay kit (GE Healthcare). The antibodies were obtained from Cell Signaling Technology (Beverly, MA, USA).

Soft agar colony formation assay. The lower layer of 0.5% agar in DMEM was placed in a 35-mm dish and permitted to solidify at room temperature. Then, 1.5×10^4 cells were suspended in the upper layer of 0.35% agar in DMEM containing 10% calf serum. The number of colonies over 50 μm was counted at 2 weeks after plating.

Statistical analysis. The results are presented as the means ± SEM. Associations were tested using the Student *t*-test and the Fisher exact test. $P < 0.05$ was considered statistically significant.

Results

Reduced 5-hydroxymethylcytosine in human tumor tissues. First, to examine the specificity of the antibody against 5-hmC, mouse liver tissues were stained with it. The signal was detected in the cell nuclei as expected, and the addition of 5-hmC-containing DNA to the reaction reduced the signal remarkably, indicating that the antibody specifically recognizes 5-hmC (Fig. 1A). Then, we performed immunostaining of human tumor and normal tissues. As shown in Figure 1(B), the signal of 5-hmC was scarcely detected in tumors compared to normal tissues, including colon, liver, brain, kidney, skeletal muscle and lung (Fig. 1B), suggesting that the loss of 5-hmC is a common phenomenon in tumorous tissues. We showed a representative photograph indicating the difference in the level of 5-hmC between the tumors and adjacent tissues derived from the mouse hepatic-tumor model (Fig. S1).[33]

Semiquantitative measurement of 5-hmC in gastrointestinal cancers. To evaluate the 5-hmC amount in many clinical specimens, the specificity of this antibody was also confirmed in blotting experiments (Fig. 2A). Serial dilution of genomic DNA extracted from mouse ES cells, in which a certain level of 5-hmC is detected,[14] were subjected to dot blot analysis. The good linearity between the signal density and DNA amount in a sufficient dynamic range supported the usefulness of this method for the quantification of 5-hmC in genomic DNA samples (Fig. 2B). Consistent with the previous report that the amount of 5-hmC decreases through differentiation in mouse ES cells,[14] the dot blot analysis demonstrated a significant loss of 5-hmC level in ES cells after withdrawal of leukemia inhibitory factor (LIF) (Fig. 2C).

Next, to assess the amount of 5-hmC in colorectal cancers (CRCs), clinical samples of human CRC obtained from surgical resection ($n = 22$ cases) were subjected to analysis. To compare the level of 5-hmC in tumors and the adjacent non-tumorous tissues, undiluted and twofold diluted DNA samples were spotted on the same membrane (Figs 2D,S2A). According to the dot blotting results, we classified the tumors into three groups: "5-hmC reduced" or "5-hmC increased" tumors were defined when the level of 5-hmC was 1/2-fold decreased (Fig. S2B) or twofold increased compared to the non-tumorous tissues, respectively. Others were classified into a "5-hmC equivalent" group (Fig. S2C). Notably, many of the CRC tumors (72.7% [16/22]) were included in the "5-hmC-reduced" group, with the others in the "5-hmC-equivalent" group (Fig. 2E). There was no distinct clinical features in 5-hmC-

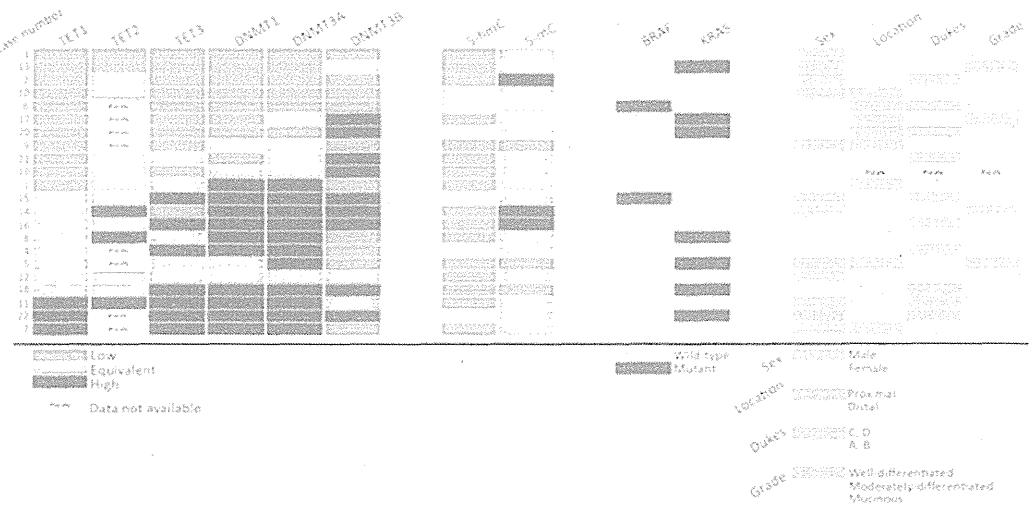

Fig. 3. Gene expressions, presence of mutations, and covariate status of 22 colorectal cancers (CRCs). Clinicopathological and molecular factors of 22 CRCs were displayed on a heat map representing *TET1*, *TET2*, *TET3*, *DNMT1*, *DNMT3A* and *DNMT3B* gene expression, and 5-hmC and 5-mC levels compared to adjacent background tissues. Presence of *BRAF* and *KRAS* mutations and covariate status of each tumor are also shown. Location: site of the primary tumor. Dukes: Dukes classification of the tumor. Grade: pathological tumor grade system.

doi: 10.1111/j.1349-7006.2012.02213.x

Table 1. Correlation between *TET1* gene expression and clinicopathological and molecular factors in colorectal cancer

Characteristics	Total $n = 22$	*TET1* expression		*P*-value
		Downregulated $n = 11$	Upregulated/ equivalent $n = 11$	
Age at surgery				
Mean ± SD (years)	65.3 ± 13.0	62.5 ± 13.4	67.8 ± 12.7	0.363
Range (years)	39–88	39–81	50–88	
Sex, *n* (%)				
Male	12 (54.5)	5 (45.5)	7 (63.6)	0.392
Female	10 (45.5)	6 (54.5)	4 (36.4)	
Site of tumor, *n* (%)				
Proximal	8 (38.1)	6 (60.0)	2 (18.2)	0.049
Distal	13 (61.9)	4 (40.0)	9 (81.8)	
Dukes grade, *n* (%)				
A, B	11 (52.4)	6 (60.0)	5 (45.5)	0.505
C, D	10 (47.6)	4 (40.0)	6 (54.5)	
Tumor grade, *n* (%)†				
Well diff	4 (19.0)	2 (20.0)	2 (18.2)	0.916
Moderately diff and mucinous	17 (81.0)	8 (80.0)	9 (81.8)	
KRAS exon 2, *n* (%)				
Wild-type	15 (68.2)	8 (72.7)	7 (63.6)	0.647
Mutant	7 (31.8)	3 (27.3)	4 (36.4)	
BRAF exon 15, *n* (%)				
Wild-type	20 (90.9)	10 (90.9)	10 (90.9)	1
Mutant	2 (9.1)	1 (9.1)	1 (9.1)	
TET2 gene expression, *n* (%)				
Downregulated	2 (14.3)	2 (28.6)	0 (0.0)	0.127
Upregulated or equivalent	12 (85.7)	5 (71.4)	7 (100)	
TET3 gene expression, *n* (%)				
Downregulated	10 (45.5)	9 (81.8)	1 (9.1)	**0.0006**
Upregulated or equivalent	12 (54.5)	2 (18.2)	10 (90.9)	
DNMT1 gene expression, *n* (%)				
Downregulated	8 (36.4)	8 (72.7)	0 (0.0)	**0.0004**
Upregulated or equivalent	14 (63.6)	3 (27.3)	11 (100)	
DNMT3A gene expression, *n* (%)				
Downregulated	7 (31.8)	6 (54.5)	1 (9.1)	**0.022**
Upregulated or equivalent	15 (68.2)	5 (45.5)	10 (90.9)	
DNMT3B gene expression, *n* (%)				
Downregulated	10 (45.5)	6 (54.5)	4 (36.4)	0.392
Upregulated or equivalent	12 (54.5)	5 (45.5)	7 (63.6)	
5-hmC level, *n* (%)				
Reduced	16 (72.7)	8 (72.7)	8 (72.7)	1
Equivalent	6 (27.3)	3 (27.3)	3 (27.3)	
5-mC level, *n* (%)				
Reduced or equivalent	19 (86.4)	10 (90.9)	9 (81.8)	0.534
Increased	3 (13.6)	1 (9.1)	2 (18.2)	

†Tumor grade: diff, differentiated. Significant *P*-values (< 0.05) are shown in bold.

reduced tumors; however, 63% (10/16) were located in the distal colon. These results were consistent with the finding that 5-hmC levels commonly decrease in neoplasms (Fig. 1B). The 5-hmC level was also reduced in the majority of gastric cancer specimens: 75% (9/12) (Fig. S3A,B).

Analysis of ten–eleven translocation (TET) and DNMT family genes expression in colorectal cancers. Given that the global level of 5-methylcytosine (5-mC) is frequently reduced in CRC tumors, we investigated whether the decrease in 5-hmC is simply due to the smaller amount of substrates, 5-mC. Then, the dot blot analysis using the anti-5-mC antibody was performed with the same sample sets applied to 5-hmC quantification, based on the specificity of the anti-5-mC antibody (Fig. S4A). Different from 5-hmC, the 1/2-fold decrease of 5-mC was detected in only 13.6% of cases (3/22), and the level of 5-mC was equivalent in most cases (72.7% [16/22]) (Fig. S4B, C). These findings indicate that the reduction of 5-hmC level in the CRC tumors is not always due to the lower amounts of 5-mC.

Recent studies indicate that the TET family of proteins can catalyze the conversion of 5-mC of DNA to 5-hmC in mammalian cells.[14,15] We suspected that the expression patterns of *TET* family genes or *DNMT* family genes encoding DNA methyltransferases affect the 5-hmC level in CRC samples. The expression of *TET1*, *2* and *3* and *DNMT1*, *3A* and *3B* was examined using quantitative real-time PCR. When we set a cut-off as twofold change, *TET1* expression was decreased in half of the tumors (50%[11/22]) and a large part of them (73% [8/11]) demonstrated less 5-hmC compared to the adjacent tissues (Fig. 3). We found that *TET2* mRNA expression was very

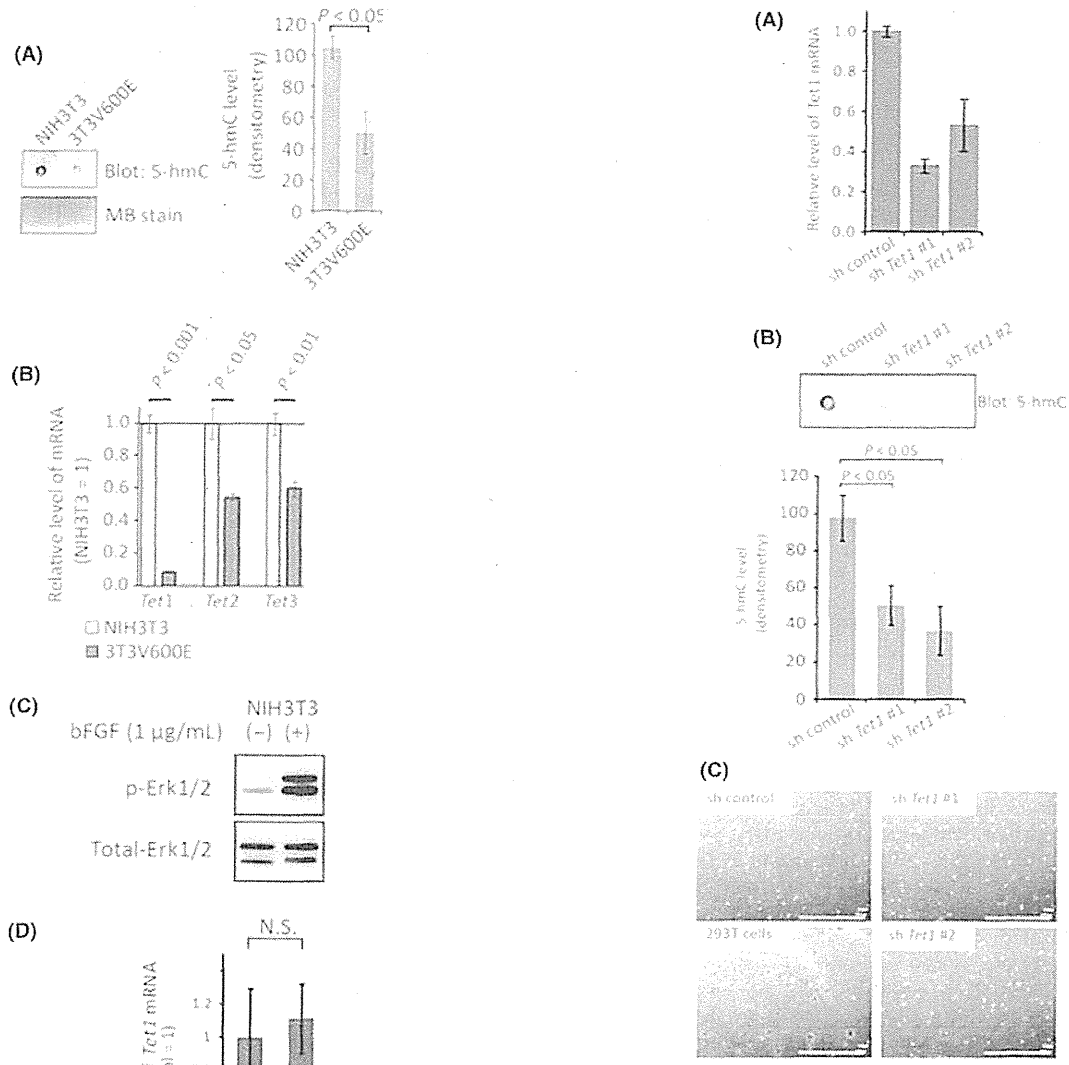

Fig. 4. 5-hmC levels and ten–eleven translocation (TET) genes expression in transformed NIH3T3 cells. (A) Genomic DNA (20 ng) of wild-type (NIH3T3) and transformed (3T3V600E) cells were subjected to dot blot analysis for 5-hmC detection. Methylene blue (MB) staining is used for DNA loading control. The graph shows the average of signals of three independent experiments. (B) Quantification of *Tet* family genes expression using quantitative RT-PCR in NIH3T3 cells and 3T3V600E cells. $n = 3$/each group. (C) Phosphorylation of Erk1/2 and (D) *Tet1* gene expression in response to bFGF stimulation for 30 min on NIH3T3 cells. NS, not significant. $n = 3$/each group.

Fig. 5. Colony formation assay on *Tet1* stably knockdowned NIH3T3 cells. (A) Knockdown of *Tet1* in NIH3T3 cells was confirmed at mRNA levels. (B) 5-hmC levels in *Tet1*-depleted NIH3T3 cells (sh *Tet1* #1 and #2) were determined by dot blot and quantified by densitometry. $n = 3$/each group. (C) Neither line of *Tet1*-depleted NIH3T3 cells acquired colony forming ability. 293T cells were used as positive control for colony formation. Scale bar, 1 mm.

little both in CRC tumors and non-tumorous tissues, and that reduced *TET1* expression was tightly associated with decreased *TET3* mRNA ($P < 0.0006$) (Table 1). In contrast, most of 5-hmC-reduced tumors without *TET1* gene downregulation showed enhanced expression of *DNMT* genes (88%[7/8]) (Fig. 3). Although the reason why the upregulation of *DNMT* genes is associated with the loss of 5-hmC is unknown, it is likely that various mechanisms, including suppression of *TET1*, affect the level of 5-hmC in CRC tumors.

Next, we examined the expression level of genes implicated in the removal of 5-hmC. Poly ADP-ribose polymerase 1 (PARP1) and APEX1 are critical components of base excision repair (BER), and activation-induced cytidine deaminase and apolipoprotein B mRNA editing enzyme, catalytic polypeptide-like 2 (APOBEC2) are deaminases, of which overexpression are reported to enhance demethylation of 5-hmC.[20] As a result, the expression of *APEX1* gene was relatively, but not statistically, high in the tumors with low levels of 5-hmC (Fig. S5).

Reduced *Tet1* expression during cellular malignant transformation. Our data in clinical samples indicated a possibility that reduced 5-hmC is associated with malignant transformation. To address this notion, we performed an *in vitro* assay using NIH3T3 cells. We previously reported that the NIH3T3 cells stably expressing oncogenic *BRAF* (V600E)

doi: 10.1111/j.1349-7006.2012.02213.x

(3T3V600E cells) acquire transformation capability.[32] In the 3T3V600E cells, the level of 5-hmC was significantly decreased when compared to control cells (Fig. 4A). The expression level of *Tet1*, *Tet2* and *Tet3* was also reduced in the 3T3V600E cells compared to the control cells (Fig. 4B). To exclude the possibility that the downregulation of these genes is directly caused by the activation of MAPK signaling itself, we treated NIH3T3 cells with bFGF and analyzed the expression of *Tet1* gene. As shown in Figure 4(C), the activity of MAPK was clearly enhanced by the treatment of bFGF; however, the expression of *Tet1* was not affected (Fig. 4D). These findings indicated that the level of *Tet1* mRNA and 5-hmC was decreased in the process of cellular transformation in NIH3T3 cells.

Reduced *Tet1* expression itself is not sufficient for cellular transformation. The above data encouraged us to expect that the decrease of Tet1 plays a certain role in the mechanism of cellular transformation. Then, to examine whether the loss of Tet1 is sufficient for cellular transformation, we established *Tet1* stably knockdowned NIH3T3 cells (Tet1KD NIH3T3 cells) using lentiviral-vector shRNA (Fig. 5A). Tet1KD NIH3T3 cells showed a decreased 5-hmC level compared to control cells (Fig. 5B). When the Tet1KD NIH3T3 cells were applied to colony formation assay, the cells did not demonstrate the colony-forming ability (Fig. 5C), suggesting that the suppression of only *Tet1* mRNA is not enough for oncogene-induced cellular transformation.

Discussion

A previous report showed that myeloid tumors with *TET2* gene mutations compromising the catalytic activity displayed lower levels of 5-hmC when compared to bone marrow samples from healthy controls.[26,27] The finding suggests a possibility that lower 5-hmC might be preferable for the emergence of leukemic cells. In solid tumors, one study revealed using immunohistochemistry that 5-hmC levels were reduced in the carcinomas of prostate, breast and colon;[30] however, the analysis using commercial tissue arrays did not compare the 5-hmC level between tumors and adjacent normal tissues. Here, we provided confirmatory evidence of 5-hmC loss in solid cancers by analyzing paired matched tissues. Also, we established the semi-quantitative assay for 5-hmC using dot blotting.

Based on data from HPLC, global hypomethylation of cytosine is widely accepted as a characteristic of malignancies, including CRC.[1,2] Since this study was based on the dot blot technique with a relatively narrow window of sensitivity, the difference in global 5-mC level might be barely observed (Fig. S4B,C). Nonetheless, the difference in 5-hmC level was obvious in most of the tumors, suggesting that loss of 5-hmC is not just a secondary effect of global DNA hypomethylation in tumors. So far, the mutation of TET family genes abrogating the demethylating activity has not been found in solid cancers;[34] however, our data suggest that there are mechanisms causing loss of 5-hmC in solid tumors.

As a mechanism for loss of 5-hmC in CRC, we demonstrated the downregulation of *TET* genes (Fig. 3 and Table 1). This is reasonable because they encode the proteins catalyzing the conversion from 5-mC to 5-hmC. Our data also suggest the existence of another mechanism underlying the 5-hmC reduction because only half of CRC showed low expression of *Tet* mRNA. The other tumors demonstrated higher expression of *DNMT* genes. One possibility is that DNMT proteins functionally compete with TET proteins on DNA strands as reported.[35] IDH1 and IDH2 generate α-ketoglutarate, on which TET depend for their enzymatic activity. *IDH* mutations specifically produce 2-hydroxylglutarate and impair the TET2 catalytic function in leukemic cells.[36] The mutant *IDH1* and *IDH2* existed exclusively with *TET2* loss-of-function mutations in acute myeloid leukemia, which suggested that the mutations of their genes are functionally similar.[36,37] Therefore, it is likely that *IDH* mutants, which are also found in CRC,[38] induce the loss of 5-hmC regardless of the normal level of *TET* genes.

In addition, we cannot exclude the possibility that elimination of 5-hmC is enhanced by the active growth of cancer cells.[22] It is possible that enhanced proliferation leads to a "passive" 5-hmC reduction because the maintenance of methylcytosine catalyzed via DNMT1 is prevented by hydroxymethylation of the target cytosine.[39] Moreover, it is reported that BER proteins and the AID/APOBEC family mediate the demethylation of 5-hmC,[20,21] and that 5-hmC is further oxidized to 5-formylcytosine or 5-carboxylcytosine by TET proteins.[17,18] We cannot exclude the possibility that the increased expression of *APEX1* mRNA is implicated in the reduction of 5-hmC in tumor cells (Fig. S5), and we intend to analyze this possibility in future research.

Our *in vitro* data demonstrated that *TET1* was downregulated in the process of cellular transformation. Given the reports that TET1 is involved in the decision of ES cell lineage specification,[15,16] the downregulation of TET1 might achieve epigenetic profiles favorable for transformation. It is not clear whether TET function is always dependent of DNA demethylating activity. Indeed, we demonstrated that tumors with low *TET* expression did not always show lower 5-hmC. It is noteworthy that TET1 directly binds to transcriptional machinery,[40] and that TET can prevent DNMT activity without DNA demethylation.[35] Hence, it is still unknown whether TET1 can play roles in cellular transformation in the enzymatic activity-independent manner. Finally, the biological significance of the loss of 5-hmC in tumors remains to be elucidated; however, loss of 5-hmC could be a diagnostic marker for malignant transformation.

Acknowledgments

We thank Dr Teiji Motojima (Division of Abdominal Surgery, Motojima General Hospital, Gumma, Japan) and Dr Takaaki Sano (Division of Pathology, Motojima General Hospital) for providing human tissue specimens. We also thank Mitsuko Tsubouchi of our laboratory for technical assistance.

Disclosure Statement

The authors have no conflict of interest.

References

1 Feinberg AP, Vogelstein B. Hypomethylation distinguishes genes of some human cancers from their normal counterparts. *Nature* 1983; **301**: 89–92.
2 Gama-Sosa MA, Slagel VA, Trewyn RW *et al.* The 5-methylcytosine content of DNA from human tumors. *Nucleic Acids Res* 1983; **11**: 6883–94.
3 Jones PA, Baylin SB. The fundamental role of epigenetic events in cancer. *Nat Rev Genet* 2002; **3**: 415–28.
4 Herman JG, Baylin SB. Gene silencing in cancer in association with promoter hypermethylation. *N Engl J Med* 2003; **349**: 2042–54.
5 Ushijima T. Detection and interpretation of altered methylation patterns in cancer cells. *Nat Rev Cancer* 2005; **5**: 223–31.
6 Jones PA, Laird PW. Cancer epigenetics comes of age. *Nat Genet* 1999; **21**: 163–7.
7 Baylin SB, Herman JG. DNA hypermethylation in tumorigenesis: epigenetics joins genetics. *Trends Genet* 2000; **16**: 168–74.

8 Herman JG. Hypermethylation of tumor suppressor genes in cancer. *Semin Cancer Biol* 1999; **9**: 359–67.
9 Ushijima T, Nakajima T, Maekita T. DNA methylation as a marker for the past and future. *J Gastroenterol* 2006; **41**: 401–7.
10 Sun L, Hui AM, Kanai Y, Sakamoto M, Hirohashi S. Increased DNA methyltransferase expression is associated with an early stage of human hepatocarcinogenesis. *Jpn J Cancer Res* 1997; **88**: 1165–70.
11 Peng DF, Kanai Y, Sawada M *et al.* Increased DNA methyltransferase 1 (DNMT1) protein expression in precancerous conditions and ductal carcinomas of the pancreas. *Cancer Sci* 2005; **96**: 403–8.
12 Nakagawa T, Kanai Y, Saito Y, Kitamura T, Kakizoe T, Hirohashi S. Increased DNA methyltransferase 1 protein expression in human transitional cell carcinoma of the bladder. *J Urol* 2003; **170**: 2463–6.
13 Ley TJ, Ding L, Walter MJ *et al.* DNMT3A mutations in acute myeloid leukemia. *N Engl J Med* 2010; **363**: 2424–33.
14 Tahiliani M, Koh KP, Shen Y *et al.* Conversion of 5-methylcytosine to 5-hydroxymethylcytosine in mammalian DNA by MLL partner TET1. *Science* 2009; **324**: 930–5.
15 Ito S, D'Alessio AC, Taranova OV, Hong K, Sowers LC, Zhang Y. Role of Tet proteins in 5mC to 5hmC conversion, ES-cell self-renewal and inner cell mass specification. *Nature* 2010; **466**: 1129–33.
16 Koh KP, Yabuuchi A, Rao S *et al.* Tet1 and Tet2 regulate 5-hydroxymethylcytosine production and cell lineage specification in mouse embryonic stem cells. *Cell Stem Cell* 2011; **8**: 200–13.
17 Ito S, Shen L, Dai Q *et al.* Tet proteins can convert 5-methylcytosine to 5-formylcytosine and 5-carboxylcytosine. *Science* 2011; **333**: 1300–3.
18 He YF, Li BZ, Li Z *et al.* Tet-mediated formation of 5-carboxylcytosine and its excision by TDG in mammalian DNA. *Science* 2011; **333**: 1303–7.
19 Ooi SK, Bestor TH. The colorful history of active DNA demethylation. *Cell* 2008; **133**: 1145–8.
20 Guo JU, Su Y, Zhong C, Ming GL, Song H. Hydroxylation of 5-methylcytosine by TET1 promotes active DNA demethylation in the adult brain. *Cell* 2011; **145**: 423–34.
21 Cortellino S, Xu J, Sannai M *et al.* Thymine DNA glycosylase is essential for active DNA demethylation by linked deamination-base excision repair. *Cell* 2011; **146**: 67–79.
22 Inoue A, Zhang Y. Replication-dependent loss of 5-hydroxymethylcytosine in mouse preimplantation embryos. *Science* 2011; **334**: 194.
23 Kriaucionis S, Heintz N. The nuclear DNA base 5-hydroxymethylcytosine is present in Purkinje neurons and the brain. *Science* 2009; **324**: 929–30.
24 Szwagierczak A, Bultmann S, Schmidt CS, Spada F, Leonhardt H. Sensitive enzymatic quantification of 5-hydroxymethylcytosine in genomic DNA. *Nucleic Acids Res* 2010; **38**: e181.
25 Song CX, Szulwach KE, Fu Y *et al.* Selective chemical labeling reveals the genome-wide distribution of 5-hydroxymethylcytosine. *Nat Biotechnol* 2011; **29**: 68–72.
26 Delhommeau F, Dupont S, Della Valle V *et al.* Mutation in TET2 in myeloid cancers. *N Engl J Med* 2009; **360**: 2289–301.
27 Ko M, Huang Y, Jankowska AM *et al.* Impaired hydroxylation of 5-methylcytosine in myeloid cancers with mutant TET2. *Nature* 2010; **468**: 839–43.
28 Moran-Crusio K, Reavie L, Shih A *et al.* Tet2 loss leads to increased hematopoietic stem cell self-renewal and myeloid transformation. *Cancer Cell* 2011; **20**: 11–24.
29 Quivoron C, Couronne L, Della Valle V *et al.* TET2 inactivation results in pleiotropic hematopoietic abnormalities in mouse and is a recurrent event during human lymphomagenesis. *Cancer Cell* 2011; **20**: 25–38.
30 Haffner MC, Chaux A, Meeker AK *et al.* Global 5-hydroxymethylcytosine content is significantly reduced in tissue stem/progenitor cell compartments and in human cancers. *Oncotarget* 2011; **2**: 627–37.
31 Ohta M, Seto M, Ijichi H *et al.* Decreased expression of the RAS-GTPase activating protein RASAL1 is associated with colorectal tumor progression. *Gastroenterology* 2009; **136**: 206–16.
32 Ikenoue T, Hikiba Y, Kanai F *et al.* Functional analysis of mutations within the kinase activation segment of B-Raf in human colorectal tumors. *Cancer Res* 2003; **63**: 8132–7.
33 Kudo Y, Tanaka Y, Tateishi K *et al.* Altered composition of fatty acids exacerbates hepatotumorigenesis during activation of the phosphatidylinositol 3-kinase pathway. *J Hepatol* 2011; **55**: 1400–8.
34 Abdel-Wahab O, Mullally A, Hedvat C *et al.* Genetic characterization of TET1, TET2, and TET3 alterations in myeloid malignancies. *Blood* 2009; **114**: 144–7.
35 Xu Y, Wu F, Tan L *et al.* Genome-wide regulation of 5hmC, 5mC, and gene expression by Tet1 hydroxylase in mouse embryonic stem cells. *Mol Cell* 2011; **42**: 451–64.
36 Figueroa ME, Abdel-Wahab O, Lu C *et al.* Leukemic IDH1 and IDH2 mutations result in a hypermethylation phenotype, disrupt TET2 function, and impair hematopoietic differentiation. *Cancer Cell* 2010; **18**: 553–67.
37 Prensner JR, Chinnaiyan AM. Metabolism unhinged: IDH mutations in cancer. *Nat Med* 2011; **17**: 291–3.
38 Yen KE, Bittinger MA, Su SM, Fantin VR. Cancer-associated IDH mutations: biomarker and therapeutic opportunities. *Oncogene* 2010; **29**: 6409–17.
39 Valinluck V, Sowers LC. Endogenous cytosine damage products alter the site selectivity of human DNA maintenance methyltransferase DNMT1. *Cancer Res* 2007; **67**: 946–50.
40 Williams K, Christensen J, Pedersen MT *et al.* TET1 and hydroxymethylcytosine in transcription and DNA methylation fidelity. *Nature* 2011; **473**: 343–8.

Supporting Information

Additional Supporting Information may be found in the online version of this article:

Fig. S1. Immunostaining of 5-hmC in the genetic model of murine hepatic tumor.

Fig. S2. Definition and determination of 5-hmC or 5-mC level using dot blot analysis.

Fig. S3. Measurement of 5-hmC in human gastric cancers using dot blot.

Fig. S4. Measurement of 5-mC in colorectal cancer (CRC) using dot blot.

Fig. S5. Expression levels of genes encoding base excision repair proteins and cytidine deaminases of 22 colorectal cancers (CRC).

Table S1. Primer sequences for quantitative real-time PCR analysis.

Table S2. Primers for mutational analysis.

Please note: Wiley-Blackwell are not responsible for the content or functionality of any supporting materials supplied by the authors. Any queries (other than missing material) should be directed to the corresponding author for the article.

doi: 10.1111/j.1349-7006.2012.02213.x

J Gastroenterol (2012) 47:477–485
DOI 10.1007/s00535-011-0512-9

ORIGINAL ARTICLE—LIVER, PANCREAS, AND BILIARY TRACT

Value of post-vascular phase (Kupffer imaging) by contrast-enhanced ultrasonography using Sonazoid in the detection of hepatocellular carcinoma

Eriko Goto · Ryota Masuzaki · Ryosuke Tateishi · Yuji Kondo · Jun Imamura · Tadashi Goto · Hitoshi Ikeda · Masaaki Akahane · Shuichiro Shiina · Masao Omata · Haruhiko Yoshida · Kazuhiko Koike

Received: 17 August 2011 / Accepted: 20 November 2011 / Published online: 27 December 2011

Abstract
Background We evaluated the sensitivity and specificity of post-vascular phase (Kupffer imaging) by contrast-enhanced ultrasonography (CEUS) using perflubutane microbubbles (Sonazoid) in comparison with conventional B-mode ultrasonography (US) for the detection of hepatocellular carcinoma (HCC) nodules.
Methods A total of 100 treatment-naïve HCC patients admitted at our hospital between December 2007 and June 2009 were consecutively enrolled. The sensitivity and specificity of conventional and contrast-enhanced US were evaluated on a liver segment basis using dynamic CT as a reference standard. Movie files of conventional and enhanced US were stored separately for each segment (e.g., lateral, medial, anterior, and posterior) and reviewed randomly by two blinded readers.
Results A total of 138 HCC nodules (mean diameter 20.3 mm) were detected in 123 of 400 segments. Detection sensitivity of B-mode US was 0.837 for reader A and 0.846 for reader B, and that of CEUS was 0.732 for reader A and 0.831 for reader B. Specificity of B-mode US was 0.902 for reader A and 0.949 for reader B, and that of CEUS was 0.986 for reader A and 0.978 for reader B. CEUS false positives were mainly due to misidentification of hepatic cysts. A significant proportion of false-negative nodules are hyperechoic in B-mode US, likely because echogenicity hampers visualization of the defect in Kupffer imaging.
Conclusions Kupffer imaging by CEUS with Sonazoid showed very high specificity but rather mediocre sensitivity for HCC detection. CEUS is highly suitable for confirmatory diagnosis of HCC; however, caution should be exercised in reaching a diagnosis based only on CEUS.

Keywords Hepatocellular carcinoma · Contrast-enhanced ultrasonography · Sonazoid

Abbreviations

AFP	Alphafetoprotein
CEUS	Contrast-enhanced ultrasonography
Conventional B-mode US	Conventional B-mode ultrasonography
CT	Computed tomography
CTAP	CT during arterial portography
CTHA	CT during hepatic arteriography
CI	Confidence interval
Gd-EOB-DTPA	Gadolinium ethoxybenzyl diethylenetriamine pentaacetic acid
HBsAg	Hepatitis B surface antigen
HCC	Hepatocellular carcinoma
HCVAb	Hepatitis C virus antibody
MI	Mechanical index
STARD	The standards of reporting diagnostic accuracy

E. Goto · R. Masuzaki · R. Tateishi (✉) · Y. Kondo · J. Imamura · T. Goto · S. Shiina · H. Yoshida · K. Koike
Department of Gastroenterology, Graduate School of Medicine, The University of Tokyo, 7-3-1 Hongo, Bunkyo-ku, Tokyo 113-8655, Japan
e-mail: tateishi-tky@umin.ac.jp

H. Ikeda
Department of Clinical Laboratory, The University of Tokyo Hospital, Tokyo, Japan

M. Akahane
Department of Radiology, The University of Tokyo, Tokyo, Japan

M. Omata
Yamanashi Prefectural Hospital Organization, Kofu, Japan

SPIO-MRI	Superparamagnetic iron oxide in magnetic resonance imaging
US	Ultrasonography

Introduction

Hepatocellular carcinoma (HCC) is a common malignancy worldwide, the incidence of which is increasing in the USA and elsewhere [1–4]. Prognosis of HCC is poor unless the cancer is detected and treated at an early stage. HCC develops usually in a liver already suffering from some chronic disease, most commonly cirrhosis. Thus, early diagnosis of HCC is essential in the management of patients with chronic liver disease [5]. While initial screening for HCC is usually performed by ultrasonography (US), contrast-enhanced dynamic computed tomography (CT) is used in a confirmatory role. Hyperattenuation in the arterial phase with washout in the late phase on dynamic CT is considered a definite sign of HCC [6]. However, dynamic CT is accompanied by substantial X-ray exposure, and examination may be contraindicated by allergy to contrast material or renal dysfunction.

Sonazoid (Daiichi-Sankyo, Tokyo, Japan), a recently introduced ultrasonographic contrast agent that contains perflubutane microbubbles within a shell of phosphatidylserine (diameter 2–3 μm), has been widely used in Japan since 2007 [7, 8]. When injected intravenously, Sonazoid particles reach the liver in about 15 s, allowing the hepatic arterial vascularity to be visualized (vascular imaging). In addition, Sonazoid is taken up by Kupffer cells approximately 15 min after intravenous injection [post-vascular phase (Kupffer imaging)], which enables differentiation of benign and malignant nodules [9]. In contrast to some other ultrasonographic contrast agents, perflubutane microbubbles continue to resonate with moderate ultrasound pressure without collapsing. Thus, Kupffer imaging is stable for more than several hours, facilitating whole-liver scanning [10]. Several reports have suggested that contrast-enhanced ultrasonography (CEUS) with Sonazoid could detect HCC nodules that are not detectable by conventional B-mode US [11, 12]. These features of Sonazoid raise the possibility of one-step depiction and diagnosis of HCC using ultrasonography alone or surveillance of HCC solely by CEUS. We sought in the present study to evaluate the diagnostic ability of CEUS in Kupffer imaging using Sonazoid for HCC.

Patients and methods

Study populations

The study design was based on the principles described in the standards of reporting diagnostic accuracy (STARD) initiative [13]. A total of 100 treatment-naïve HCC patients who were admitted to the authors' institution for treatment between December 2007 and June 2009 were consecutively enrolled. Exclusion criteria were (1) patients with egg allergy or a past history of allergic reaction to Sonazoid; (2) those with HCC located in the caudate lobe; (3) those suffering severe cardiac or pulmonary dysfunction, which may affect Sonazoid delivery; and (4) those with HCC that showed an atypical dynamic CT pattern, as defined below. Data was collected prior to performance of Sonazoid CEUS.

This study was conducted according to the ethical guidelines for epidemiologic research of the Japanese Ministry of Education, Culture, Sports, Science and Technology and the Ministry of Health, Labour and Welfare. Informed consent was obtained from all patients. The study design was approved by the ethics committee of the authors' institution.

Computed tomography

HCC was diagnosed by using dynamic CT prior to enrollment; hyperattenuation in the arterial phase with washout in the late phase was considered diagnostic of HCC (Fig. 1a, b) [14]. Dynamic CT was performed less than 1 month before Sonazoid CEUS. All CT examinations were performed using a 64-detector row helical CT (Aquilion 64; Toshiba Medical, Tokyo, Japan and LightSpeed VCT; GE Health Care, Tokyo, Japan). All subjects were given an intravenous injection of nonionic contrast material at 2.0 mL/kg body weight, to a maximum of 100 mL, using a power injector (Dual Shot GX; Nemotokyorindou, Tokyo, Japan) at a rate of 3 mL/s. We used fixed scanning delays in the double-arterial phase protocol: the early arterial phase starts at 25 s, the late arterial phase at 40 s, and the equilibrium phase starts 120 s after the beginning of contrast material injection. Following this, a bolus-tracking program is used to optimize the scanning delay for dynamic imaging.

Ultrasonographic imaging

Ultrasonography was performed before initiation of treatment on an inpatient basis after at least 5 h fasting using the SSA-770A (Aplio; Toshiba, Tokyo, Japan) ultrasound apparatus. Tissue harmonic imaging (2.5/5.0 MHz, 14–27 Hz) was used in B-mode US, and Sonazoid CEUS employed phase-inversion harmonic mode [mechanical index (MI), 0.2–0.3; gain, 75–90 dB; dynamic range, 45 dB; frame rate, 15 frames/s). The focus point was set 8–10 cm from the body surface (Fig. 1c).

Ultrasonographic contrast media

For Sonazoid CEUS, one vial (16 μg) of Sonazoid (Daiichi-Sankyo, Tokyo, Japan) was reconstituted with 2 mL of